PASSIVE RANGING USING A DISPERSIVE SPECTROMETER AND OPTICAL FILTERS

THESIS

Jacob A. Martin,

AFIT-ENP-12-D-02

DEPARTMENT OF THE AIR FORCE
AIR UNIVERSITY

AIR FORCE INSTITUTE OF TECHNOLOGY

Wright-Patterson Air Force Base, Ohio

PASSIVE RANGING USING A DISPERSIVE SPECTROMETER AND
OPTICAL FILTERS

THESIS

Presented to the Faculty

Department of Engineering Physics

Graduate School of Engineering and Management

Air Force Institute of Technology

Air University

Air Education and Training Command

in Partial Fulfillment of the Requirements for the

Degree of Master of Science in Applied Physics
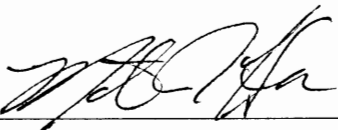
Jacob A. Martin, B.S.

December 2012

AFIT/ENP/12-D02

PASSIVE RANGING USING A DISPERSIVE SPECTROMETER AND
OPTICAL FILTERS
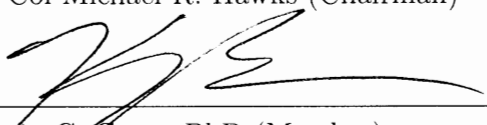
Jacob A. Martin, B.S.

Approved:

_____   ___14 DEC 12___
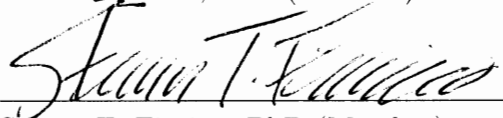Lt Col Michael R. Hawks (Chairman)   Date

_____   ___14-DEC-2012___
Kevin C. Gross, PhD (Member)   Date

_____   ___14 DEC 12___
Steven T. Fiorino, PhD (Member)   Date

AFIT-ENP-12-D-02

Abstract

Monocular passive ranging using atmospheric oxygen absorption bands has been successfully demonstrated in the past using fourier transform spectrometers. These instruments are very sensitive to vibration, however, making them difficult to use on an air or space-borne platform. This work focuses on whether passive ranging can be done with instruments that are easier to deploy. Two potential instruments are tested and compared: a diffraction grating spectrometer, as well as placing optical filters in front of a camera. A grating spectrometer was able to estimate range to within 5% for a static solid rocket motor firing from a distance of 910 m using the NIR absorption band of oxygen. Testing at shorter ranges with a lamp, on the order of tens of meters, also produced range estimates accurate to within 5% for the NIR band. The visible band was also measured by the spectrometer at these ranges, but range estimates were only accurate to within 15%. Using the sun as a source, optical filters were able to successfully measure the pathlength through the atmosphere to within 3% for both the visible and NIR bands. Testing the filters using a quartz tungsten halogen lamp as the source, however, proved unsucessful. The most likely cause of error is the source irradiance changing over time. A system is discussed and modeled in ZEMAX to potentially measure multiple filters simultaneously, which would eliminate this issue. A model was also created to predict how both techniques will scale to longer ranges. An instrument using filters is predicted to be more accurate at long ranges, but only if the grating spectrometer has to be fiber coupled to the collection optic.

Acknowledgements

Table of Contents

List of Figures

List of Tables

List of Abbreviations

PASSIVE RANGING USING A DISPERSIVE SPECTROMETER AND
OPTICAL FILTERS

I. Introduction

Developing a ballistic missile defense system has been a goal of the US military
since the early days of the Cold War. Current defense systems are only capable of
intercepting missiles in terminal or descent phase. Boost or ascent phas intercept
would enable a more robust defense, but is not currently feasible. The first require-
ment for such a system must be to develop a sensor capable of finding and tracking
the missile in flight. This sensor can be either passive or active. Passive sensors pro-
vide several advantages over traditional active sensors, such as radar. First, since no
signal is emitted, a passive sensor is much more difficult to detect, which is especially
important on stealth platforms. Additionally, detecting the signal of an active sensor
allows the target to deploy countermeasures to confuse or defeat the sensor. Finally,
the signal from an active sensor has to travel to and return from the target. This
makes detecting targets at long ranges difficult. Since passive sensors rely solely on
emission or reflections from the target, no large power source is needed to emit a
strong signal. This is especially advantageous for small platforms such as drones.

A passive sensor is particularly suited for tracking ballistic missiles. The exhaust
plume for a ballistic missile is very bright, making it highly visible even at long ranges.
Since a passive ranging sensor can detect the position of a missile soon after launch,
it's still possible to find the missile in boost phase. Being able to find and track
missiles in boost phase has several advantages. The missile is moving much slower
than during reentry, making it easier to intercept, or get the necessary dwell time

with a laser. Also, the potentially toxic debris will fall near the launch point of the missile, as opposed to over friendly nations.

The problem with current passive sensors is they are only able to determine the direction to the target. To determine the actual location of a target, multiple sensors are needed to triangulate the position. This requires time for the sensors to share their information, and for software to determine the position of each sensor to calculate the location of the target. Also, this requires more sensors, as multiple sensors will need line of sight to a given area, at all times. A passive sensor capable of also determining range will eliminate the need for multiple sensors, and allow target location to be determined almost instantaneously.

Passive sensors can take many different forms, but using atmospheric gas absorption, specifically O_2, to determine range will be discussed in this paper. There are two particular absorption bands of oxygen that have several advantages. The first band is centered at 14527 cm^{-1}, in the visible, and the second is centered at 13122 cm^{-1}, in the near infrared (NIR). Both these bands are spectrally isolated from other atmospheric absorption bands. The P-branch of the visible band partially overlaps with an absorption band of water, and there is a strong potassium doublet, a trace contaminant in solid rocket motors, emission feature in the P-branch of the NIR band. The R-branch, however, is completely spectrally isolated in both cases. This enables a baseline to be fit to determine the spectrum of the source, eliminating the need for *a priori* knowledge of the target.

Secondly, these oxygen bands are relatively weak. This allows for long pathlengths to be measured before the band becomes completely optically opaque. Third, the atmospheric concentration of oxygen is relatively stable and predictable. Because of this, detailed weather information along the entire path is not needed, which simplifies the calculation and reduces potential errors. Finally, since the bands aren't in the

LWIR or MWIR, the focal plane does not need to be cooled, which generally reduces instrument size and complexity.

1.1 Problem Statement

The purpose of this research is to demonstrate passive ranging using a dispersive grating spectrometer and optical filters, and to determine suitability of each for use in air or space-borne sensors.

II. History

The first attempt at passive ranging was done by Leonpacher at AFIT. This research focused on the CO_2 absorption feature at 4.3 μm. His technique compared the relative intensity between two spectral bands (2200-2225 cm^{-1} and 2225-2250 cm^{-1}.) The actual range estimation was done by comparing the measured intensity ratios to previously measured data for a given source at a given range. In this way, the range was only classified into a few discrete bins, as opposed to measuring an actual value of distance to target. The absorption feature used is relatively strong, so it was only successful for ranges up to 5 km. There were several problems with this method when it comes to ranging ballistic missiles, however. First, since only two bands are compared, some *a priori* knowledge of the target is required to determine what the ratio of intensities should be at a given range. Second, combustion sources often have hot CO_2 in the plume, which will emit extra light into the absorption band. This will make it appear that there is less atmospheric absorption than there actually is. Finally, since the absorption band is very strong, it is impossivle to measure pathlengths more than a few kilometers. It is highly unlikely that a ballistic missile will be this close to the sensor.[3]

The work of Draper, et al. further developed this technique to attempt to get a true value for range, as opposed to simply fitting it into a discrete interval. The basic idea is that the ratio of intensities of an in-band to out-of-band filter should fall off exponentially with range according to Beer's Law. By modeling this, and adding in factors such as the source spectrum and aerosol scattering, a relationship between the range to target and the ratio of the intensities measured through each filter can be developed. From this, range can be determined using only the measured intensities through each filter, without the need for calibration at each range. In reality, however, it was very difficult to create a good model for actual field tests, so the range estimate

results were disappointing. Additionally, this technique still has the some of the same issues as the work of Leonpacher, since a priori knowledge of the target spectrum is required. [4]

The technique of Advanced MPR was developed by OptoKnowledge Systems Inc (OKSI). This looked at the same bands, but used an imaging dispersive spectrometer instead of filters. MODTRAN was then used to determine what the atmospheric spectrum should look like at a given range to the target. An iterative process was used to determine the atmospheric absorption profile that most closely matched the measured spectrum. The spectrometer looked in the entire MWIR, making it possible to observe CO_2 features at 2 μm and 4.3 μm simultaneously. In actual testing, however, the second order diffraction overlapped with the 2 μm band, making it impossible to use. Although only the two CO_2 bands were looked at, 3 other absorption bands were identified as suitable to use for passive ranging: O_2 at .762 μm, as well as, O_3 at 4.7 μm and 9.6 μm. The problem was that the source had to be modeled for the iterations to converge to a solution. Range estimates were highly dependent on this modeling of the plume, which was difficult in practice. [5]

Passive ranging using atmospheric oxygen was first demonstrated by Hawks, at AFIT, using the NIR O_2 band centered at 762 nm. This was done using a Fourier Transform Spectrometer (FTS), comparing the average intensity measured at points in the oxygen band, and comparing it to a baseline determined from the spectrum measured out the absorption band. The absorption is taken as the difference between the baseline fit and the measured spectra across the absorption band then averaged over the entire band. FASCODE was used to determine what the band average absorption should be at various ranges, to develop a function of absorption versus range. The measured absorption is then compared to the absorption versus range curve to determine the range. This was successfully demonstrated at ranges up to

5

3 km. Additionally, the technique was predicted, based on models, to be capable of working at hundred of kilometers. The spectrometer used, however, is very sensitive to vibration, making it almost impossible to deploy on an air or space-borne platform. [6]

Work was also done at AFIT by MacDonald to use band average absorption on CO_2 absorption bands. Calculations were made using previously measured spectra of explosive fireballs. This work focused on the CO_2 feature at 2.0 μm, which was chosen because there is minimal background from atmospheric emission and solar scattering. This technique was quite successful as measured ranges were within 3% of the true value for ranges up to 5 km. Additionally, this method was predicted to work for ranges up to 50 km. When tracking ballistic missiles, however, it is desirable to measure ranges out to hundreds of kilometers, making this technique somewhat limited in that application. [7]

One attempt to demonstrate passive ranging using oxygen, with a deployable sensor, was tried by Anderson at AFIT in 2010. This used an Acousto-Optical Tuneable Filter in front of a PIMAX Intensified CCD (ICCD) camera. The filter was tuned to three separate spectral bands: two out of the absorption band centered at 778 nm and 752 nm, and one centered in the absorption band at 762 nm. The intensity was measured through each band and a baseline was fit to the two out-of-band intensities. This provides fewer points to calculate a baseline, and in-band intensity, compared to an FTS. It is, however, capable of being deployed in a tactical environment. The absorption measurements were quite noisy, making it difficult to accurately determine range. One problem was that it took time for the filter to stabilize while changing between bands. This makes measuring absorption for a source with a temporally varying irradiance nearly impossible. [8]

The most recent development was demonstrating passive ranging can work on

6

moving targets, done by Vincent at AFIT in 2011. Additionally, it was demonstrated that the visible oxygen band, centered near 690 nm, can be used for passive ranging, also using an FTS. The measured spectrum was noisy, however, and led to large errors (often greater than 20%) in measured range. The visible band was found to be less accurate than the NIR band at short ranges. In testing done at a range of 13 km, however, the visible band gave far more accurate range estimates than the NIR band. This is expected because the visible band is weaker. Therefore, at short ranges the absorption measured is so small it is more affected by noise. At long ranges, however, the visible band works better because it allows for larger pathlengths before the band becomes optically opaque. [9]

III. Theory

3.1 Spectroscopy

Because the O_2 molecule is homogeneous and diatomic, it has no dipole moment. There are, however, magnetic dipole allowed transitions, which are much weaker than electric dipole transitions. On average, magnetic dipole transitions are about 10^5 times weaker than electric dipole allowed transitions. As discussed earlier, weak transitions are desirable for passive ranging, because they allow long path lengths before saturating. The specific transition observed for this work is the O_2 $X \rightarrow b$ transition, which is centered at 13122 cm^{-1}. This is a magnetic dipole allowed transition. In addition, because this is a singlet-triplet intercombination, it is even weaker than average magnetic dipole transitions. The transition moment for this band is only 0.14 s^{-1}. There is also an overtone corresponding to the v''=0 $\rightarrow$ v''=1 transition, which is centered at 14527 cm^{-1}. Because the ground state of this transisition is less populated, it is even weaker than the NIR band allowing even larger pathlengths than the NIR band before the band becomes optically opaque. [10]

Figure 1 shows the individual lines of various atmospheric gases, with their relative strengths, taken from the HITRAN database. The line strengths are scaled by their atmospheric abundance at 0 altitude, using the US Standard Atmosphere. Oxygen is shown in green, while water is shown in black (color copy available in digital format.) Additionally, there are HCl, OH, and CO_2 absorption bands in this spectral region, but they are too weak to be visible on this scale. The R-branches of both oxygen absorption bands are spectrally isolated from other atmospheric gases. Also, both bands have a large spectral region near them with no atmospheric absorption, which can be used to establish a baseline. It's also clear the NIR band is much stronger than the visible band. [11]
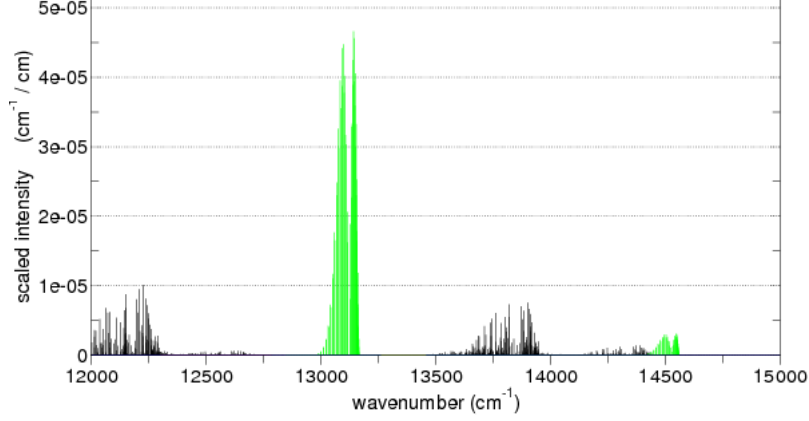
Figure 1. Spectral lines of oxygen (in green) and water (in black) taken from the HITRAN database. The relative line strengths are scaled by their atmospheric abundance.

3.2 Band Average Absorption

The basic principle of MPR relies on Beer's Law,

$$I\left(v\right) = I_0\left(v\right)e^{-k(v)L}, \tag{1}$$

where k is the aborption coefficient and L is the pathlength. $\frac{I(v)}{I_0(v)}$ gives the fractional tranmission, at a given wavelength, through the atmosphere. One minus the fractional transmission gives the fractional absoption,

$$A\left(v\right) = 1 - T\left(v\right) = 1 - \frac{I\left(v\right)}{I_0\left(v\right)} = 1 - e^{-k(v)L}. \tag{2}$$

Here, $k\left(v\right)$ depends on both the properties of molecules within the atmosphere, as well as, their number density, and can be expressed as $k = \sigma\left(v, P, T\right)N\left(P, T\right)$, where $\sigma\left(v, P, T\right)$ is the absorption cross section and $N\left(P, T\right)$ is the number density of the specific molecule. Both σ and N depend of weather conditions, specifically pressure and temperature. These factors can be approximated from atmospheric modeling. The cross sections for individual molecules, as a function of temperature and pressure,
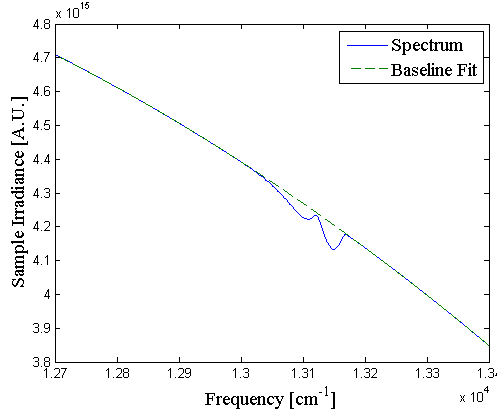
Figure 2. This shows a sample spectrum, I, with an absorption band. The dashed line represents the baseline or I_0.

are provided by the high-resolution transmission molecular absorption (HITRAN) database.

Since both σ and N are known, the pathlength through the atmosphere can be determined from estimates of absorption. In order to do this, $\frac{I(v)}{I_0(v)}$ must be measured. Because both O_2 bands are spectrally isolated from other atmospheric absoption features, a baseline can be fit to the spectrum outside absorption band. This can be used to approximate $I_0(v)$ within the absorption band. $I(v)$ is then measured, making it possible to calculate an absorption, and thus a pathlength. A basic example of this is shown in Figure 2.

In reality, it is very difficult to measure individual lines with simple instruments, so instead the average absorption over the band is taken. In addition to making absorption easier to measure, averaging over the entire band reduces the temperature dependence of the absorption measurement. The strength of individual lines is going to depend on how population of the energy state corresponding to that transition, which will change with temperature. Since the entire band is averaged over, there will be a fixed population based only on the pathlength. There will still be some temperature dependence , however, because the concentration of O_2 will vary with temperature. Averaging over the entire band gives the band-average transmission,

10

$$\bar{T} = \frac{1}{(v_2 - v_1)} \int_{v_1}^{v_2} T(v)\, dv. \tag{3}$$

Here, v_1 and v_2 represent either end of the absorption band. This fails to account for some factors, such as, solar scattering or the spectral response function of the instrument used to measure the spectrum. If these are assumed to vary smoothly, (i.e. they can be closely approximated by a low order polynomial) over the spectral ranges being examined, they will be accounted for in fitting the baseline. These effects will equally affect the measurement of $I_0(v)$ and $I(v)$, meaning the factor will drop out when $I_0(v)$ and $I(v)$ are divided.

3.2.1   Measuring Absorption With Filters

When using filters to measure absorption, however, the assumption that the spectral response is smoothly varying may not be accurate. This is because it's hard to design multiple filters with identical bandwidths at different wavelengths. So the flux measured through each filter must be normalized. The normalized flux is defined

$$\Phi_{norm} = \frac{\int T_f(\lambda)\, \Phi(\lambda)}{\int T_f(\lambda)}, \tag{4}$$

where T_f is the transmission function of the filter and Φ is the flux from the source at the detector. The absorption is then

$$\bar{A} = 1 - \bar{T} = 1 - \frac{\Phi_{norm,measured}}{\Phi_{norm,baseline}}. \tag{5}$$

$\Phi_{norm,measured}$ is the measured flux through the in-band filter, while $\Phi_{norm,baseline}$ is the estimate of what the flux would be if there was no atmospheric absorption.

3.3 Radiometry

Because the baseline is measured during testing, absolute radiometry is not necessary for this method of passive ranging. It is good, however, to have at least a general idea of the radiometry, to determine how this technique will scale to longer pathlengths. The spectrum of a rocket motor plume can be closely approximated by a greybody emission function. There are specific spectral features that will be addressed later, but the overall spectrum will look like a greybody. With this in mind, the spectral radiance of the plume can be approximated as:

$$L\left(\lambda, T\right) = \varepsilon * \frac{2 * 10^{18} c}{\lambda^4} * \frac{1}{e^{\frac{10^6 hc}{\lambda k T}} - 1} [\frac{photons}{m^2 \cdot sr \cdot \mu m \cdot s}], \tag{6}$$

where ϵ is the emissivity, λ is the wavelength (in μm), c is the speed of light (in m/s), h is Planck's constant, k is the Boltzmann constant, and T is the temperature of the emitter. The irradiance observed at the aperture of the sensor is then

$$E\left(\lambda, T\right) = L\left(\lambda, T\right) * T_a\left(\lambda\right) * \frac{A_s}{R^2} [\frac{photons}{m^2 \cdot \mu m \cdot s}], \tag{7}$$

where T_a is the atmospheric transmission, A_s is the area of the source (in m), and R is the distance between the sensor and the source (in m). To get this in units of photons per second, it's necessary to integrate over a wavelength band and multiply by the area of the reciever aperture. A spectral response function for either the filters or the spectrometer will have to be added to the integration to get a photon count. So, the total number of photons at the sensor aperture will be

$$N = \tau * \int E\left(\lambda, T\right) f\left(\lambda\right) QE_c\left(\lambda\right) A_d d\lambda, \tag{8}$$

where τ is the exposure time of the camera, A_d is the area of the detector, QE_c is the quantum efficiency of the camera, and f is the spectral response function of either

12

the filters, or a single pixel in the spectrometer. In general, this integration would be over all wavelengths, but since the detector used in testing was silicon based, the camera will only detect photons up to 1.1 μm.

If the sensor is shot noise limited, which is the ideal case, then the noise will be the square root of the number of photons. This means the signal to noise ratio will also be the square root of N. This will be used later, when comparing how the filters and spectrometer will scale to longer ranges. These equations do not take into account the transmission through the atmosphere, which will attenuate certain wavelengths differently than others. Also, it doesn't include the noise effects of the sensor itself, but these will be addressed later. [1]

3.4   Atmospherics

For this project, the line-by-line radiative transfer model (LBLRTM) is used to model the absorption spectrum of the atmosphere. LBLRTM uses the HITRAN database to determine the line positions and strengths for various species of gases. Each line is then convolved with a Voigt profile, based on temperature and pressure, to determine the spectral absorption. In addition, an instrument lineshape can be added, if necessary. This isn't needed when computing absorption for the filters, but is with the dispersive spectrometer, where the lineshape is the spectral response for a given pixel on the spectrometer. The program divides the pathlength into small discrete intervals. The concentration of atmospheric gases for each interval, or layer, will be found based on the temperature and pressure at that location along the path. For this project, the temperature and pressure are determined using the US standard atmosphere. The absorption is then calculated for each layer, and then absorption through each layer is multiplied to get the absorption along the entire path. LBLRTM also takes into account Rayleigh scattering. Several other choices

13

are provided to determine the concentrations of various gases in the atmosphere. For this project, however, only the 1976 US standard atmosphere is used. [12]

The concentrations will still depend on local weather conditions such as temperature and pressure, however. In order to account for this, a weather correction is used. The concentration of specific gases used in LBLRTM is given in the TAPE 6 file, which is produced every time the LBLRTM code is run. Based on weather measurements of temperature, air pressure, and humidity, a better approximation of the true concentrations can be made. In this case, the primary species of importance is oxygen. The fractional error in concentration produces an approximately equal fractional error in predicted absorption. For example, if the actual concentration is two percent lower than that used in LBLRTM the absorption prediction will be about two percent larger than it should be. The predicted absorptions would then be divided by a factor of 1.02 to adjust for this error in concentration. [6]

3.4.1 Look Angle

Because concentration drops off with altitude, it is advantageous to use an air or space-borne platform. Beer's Law states that absorption increases with concentration, meaning the light from the target will not be absorbed as quickly if it is traveling through less dense air. With a sensor at the ground, most of the light in the absorption band will be absorbed quickly, making it more difficult to measure the absorption for targets at long ranges. If the sensor is placed at a higher altitude, however, the concentration will be lower. This makes it possible to accurately measure longer pathlengths before the absorption band becomes optically opaque. Figure 3 shows how absorption varies with range for two different scenarios. The first is with the sensor at 0 altitude, and a look angle of 85 degrees off zenith. The second is for a sensor at 25 km altitude, with a look angle of 95 degrees off zenith. Both scenarios
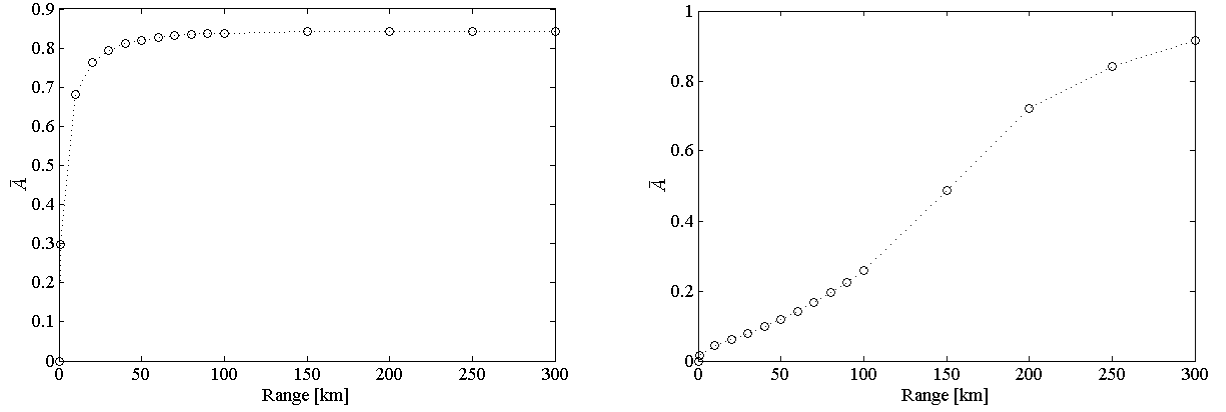
Figure 3. A side-by-side comparison of the absorption vs range curves for uplooking and downlooking sensors. In the downlooking scenario, the absorption increases much more slowly making it more useful especially at long ranges.

are using the NIR oxygen band absorption. The downlooking range curve has a larger slope after about 30 km, meaning a fixed error in absorption will translate to less error in range than in the uplooking scenario. In addition, in the downlooking scenario the absorption is almost linear with range, making it equally effective at all ranges covered.

3.4.2 Visible vs. NIR band

As discussed earlier, the visible band is weaker than the NIR band, meaning longer ranges are possible before it saturates. To demonstrate this, the same conditions as the downlooking scenario were used and applied to both the NIR and visible band. The results are shown in Figure 4. Even at 300 km, the visible band is not anywhere near optically opaque, as only about 60% of the light within the band is absorbed. The NIR band, on the other hand, is starting to tail off as it approaches 100% absorption. In this scenario, ranges much longer than 300 km are possible for the visible band, but not the NIR band.
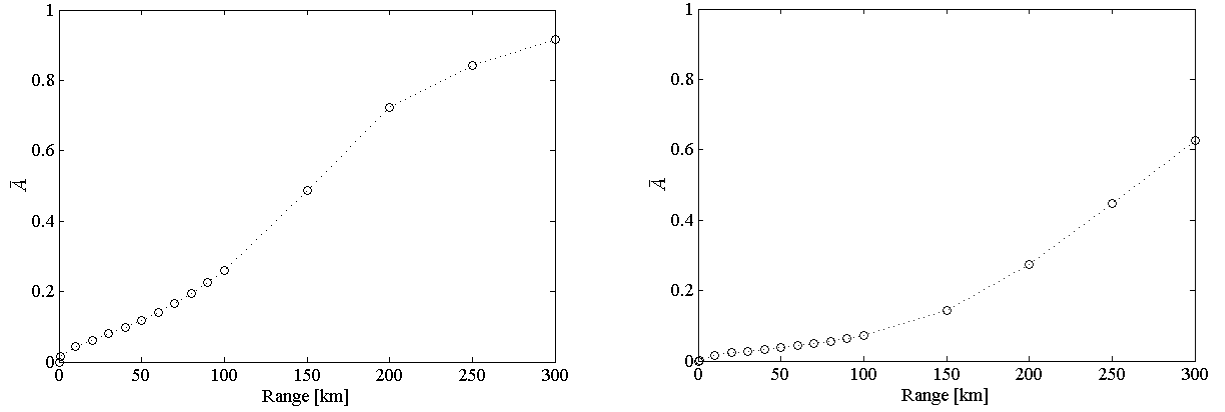
Figure 4. Comparing the visible absorption band (on the right) to the NIR band (on the left) with the same look scenario as the downlooking case shown previously.

3.5 Camera Considerations

A PIMAX 16-bit ICCD camera was used for this project. The camera works by placing a photocathode at the entrance window of the camera. When incoming photons hit this, they emit electons which are then drawn towards a microchannel plate (MCP) by an electric field. The MCP consists of many small glass channels, which the electrons are sent through. A voltage is applied across the MCP to accelerate the electrons through these channels. As the electrons accelerate, they gain energy, and begin to knock electrons out of the walls of the microchannel. This creates a beam of many electrons from just one incident electron. These electrons are then readout like in a traditional CCD array. [13]

3.5.1 Dark Noise

One issue that was encountered with this camera was the dark noise. Dark noise essentially comes from two main sources. First, thermal excitation of electrons in the CCD itself causes the camera to detect something even when a photon isn't present. In general, this isn't a big issue when dealing in the visible and NIR. The other is noise involved in reading out the data from the CCD, which is called read noise. These can

16

be mostly calibrated out, since it is a fixed offset. There is some random variation in this, however, which creates uncertainty. To get a better idea of how this affected the camera, measurements were taken with the aperture completely unilluminated while camera settings, namely gain and exposure time, were varied. Both the mean and the standard deviation were taken. The mean represents a fixed offset, which can be calibrated out. The standard deviation represents random variation, which is harder to account for. The variance in the dark noise increases with both exposure time and gain, but it never rises above 6.5 digital counts. For a 16 bit camera, this represents about .01% of the dynamic range, so it's effect is small. Still, when the measured irradiance is low, the dark noise could become a factor.

3.6   Optical Filters

Optical filters are designed based on the principle of thin film interference. When the thickness of a material is on the order of the wavelength of light, the light reflected of the front and back surfaces of the film will interfere, causing certain wavelengths of light to destructively interfere. The condition for destructive interference, assuming normal incidence angle, is

$$2nt = m\lambda, \tag{9}$$

where n is the index of refraction of the film, t is the thickness, and m is any positive integer.

When the condition for destructive interference is met, light of that wavelength will not be reflected by the film. The films are made of materials with low absorbances, so light that is not reflected will be transmitted through the film. Similarly, when constructive interference happens (replace m with m-1/2 in Equation 9), the light will be at least partially reflected, meaning less will be transmitted through. Most

wavelengths are partially transmitted, creating a sinosodial variation of transmission through the film with wavelength. By stacking a number of thin films on top of each other, it is possible to build filters that will only transmit light in certain wavelength ranges. For a finite number of layers, there will have to be some periodicity to the tranmission, but so long as the tranmission outside the desired region is 0 over the spectral response of the detector the secondary tranmission peaks don't matter. [14]

3.7   Dispersive Spectrometers

Dispersive spectrometers work by creating wavelength dependent dispersion angles, usually with either a diffraction grating or a prism. For the testing discussed in this paper, a Czerny-Turner diffraction grating spectrometer was used. A collimated beam of light is sent into the spectrometer, usually through a slit to ensure all rays hit the diffraction grating at roughly the same angle. If no entrance slit is used, the light entering the spectrometer will hit the grating at different angles. So, light of one wavelength will hit the focal plane in different locations depending on where it is coming from in the scene. This makes it difficult to determine the actual spectrum being measured. The collimated beam is then reflected off the diffraction grating creating an angular seperation.

The angular deviation off a diffraction grating is given by

$$sin\left(\theta_d\right) = sin\left(\theta_i\right) + m\frac{\lambda}{\Lambda}. \tag{10}$$

Here θ_d is the reflected angle with respect to the normal of the grating surface, θ_i is the incident angle, m is any positive integer, and Λ is the spatial period of the grooves on the grating. Taking the derivative with respect to the wavelength gives

the angular dispersion,

$$\frac{\partial \theta_d}{\partial \lambda} = \frac{m}{\Lambda cos\left(\theta_d\right)}.$$ (11)

If θ_d is assumed to be small, a first order Taylor expansion can be used to find the angular separation between two wavelengths

$$\Delta \theta = \frac{m}{\Lambda cos\left(\theta_d\left(\lambda_0\right)\right)}\left(\lambda - \lambda_0\right).$$ (12)

The new spectrally separated beam of light is then reflected off a focusing mirror, which translates the angular deviation into a linear separation at the focal plane. Each row of pixels will then give the spectral information over a range of wavelengths. Since one dimension of the focal plane array is used to measure the spectrum, the spatial information is limited to one dimension. The range of wavelengths, as well as, the spectral resolution can be varied based on the grating, the size of the focal plane array, and the focal length of the focusing mirror. The spectral resolution is limited by the Rayleigh Criterion for diffraction, but for this application that level of spectral resolution isn't necessary. [2]

IV. Spectrometer Data

For the tests in this project, a .275 m Acton Research Spectrometer was used. The grating used in testing was a 1200 groove per mm grating blazed at 750 nm. A PIMAX ICCD camera was placed at the focal plane for data collection. The spectrometer uses a fiber optic cable to bring light from the collecting optic to the spectrometer. The light from the fiber is then focused onto the entrance slit using optics attached to the spectrometer.

4.1 Road Flare Test

The first test using a dispersive spectrometer was outside of Building 194 using a road flare. The primary purpose of this test was to prepare to observe a static rocket motor firing discussed later. A road flare is good for this purpose because it contains potassium, which is a trace contaminant in solid rocket motors. The potassium D1 and D2 lines emit very strongly at 766.5 nm and 769.9 nm. This is within the P-branch of the NIR O2 band, but not in the R-branch. It is important, however, to ensure the potassium lines don't saturate and spill over into the R-branch.

The flare was placed approximately 50 m from the spectrometer. The camera was set to take 50 frames, with a 0.1 second integration time, and 0 gain. A background was also taken, with the same settings, and subtracted to reduce the effect of solar scattering. The camera was set to bin rows, meaning the CCD reported a single value for each column of pixels. For this experiment, pixel rows 400-700 were chosen because they appeared to roughly correspond to pixels illuminated by the scene. This essentially creates an average spectrum measured over the field of view of the pixels chosen to bin. The spectrometer was fiber coupled into a Vixen R200 Newtonian telescope. The measured spectrum is shown in Figure 5.
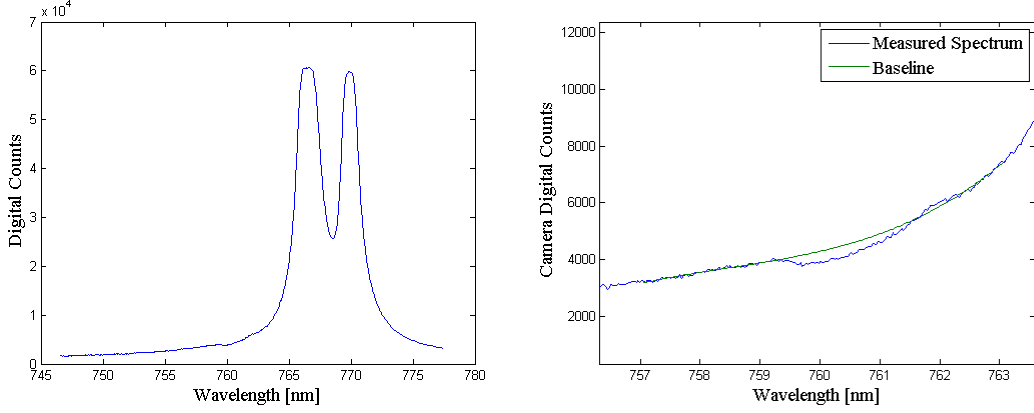
Figure 5. The measured spectrum of the road flare with background subtracted. The R-branch of the oxygen band is the small dip around pixel 450. The picture on the right is the same spectrum with a closeup of the oxygen band. The baseline fit is also drawn in.

The resulting measured absorption averaged over the NIR band was 0.045 ± 0.038. The uncertainty was estimated by taking the standard deviation of the absorption measured in each of the 50 frames. According to LBLRTM, this absorption corresponds to a range of 54 m. A plot of the measured absorption, along with the absorption versus range curve from LBLRTM, is shown in Figure 6. This represents an 8% error from the true range. Additionally, the error bars on the measurement are too large to display on this scale. This could be due to the potassium emission
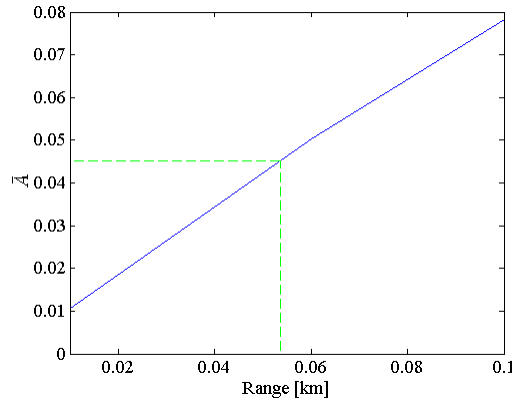
Figure 6. Predicted absorption vs range curve from LBLRTM for the flare test. The value for the measured absorption is drawn in as well.

Table 1. Summary of the camera settings used in data collection.

Trial	Integration Time (s)	Gain (A.U.)
1	0.1	150
2	0.1	255
3	0.5	255
4	0.5	255

lines. The potassium lines should be accounted for in the baseline, but it's difficult to fit a baseline with high confidence in this data.

4.2 ATK Solid Rocket Motor Test

A static firing of a GEM-40 Solid Rocket Motor (SRM) was observed at the ATK testing facility in Utah. The SRM burned for approximately 60 seconds. The rocket motor was observed from a range of approximately 910 m. The sensor was at an altitude of 1.495 km with a look angle of 96.7 degrees off zenith. Light from the plume was collected by a Meade LX-200 telescope and focused onto a fiber bundle which relayed the light to the entrance of the spectrometer. The telescope has an aperture area of 710 cm^2, however, the aperture was partially covered, to prevent the camera from saturating. The effective area was 103 cm^2 in this experiment.

Four trials of ten frames each were measured, however, the last six frames of the fourth trial occurred after burnout. The camera settings for each trial are shown in Table 1.

After the rocket burn had finished, ten frames were taken with each setting, to estimate a background. This helps reduce the error from scattering and from the dark noise of the camera. With an imaging fiber, this could be measured simultaneously with the spectrum of the rocket plume by looking at pixels in the sensor FOV but outside the rocket plume. Since the fiber used for this test was not an imaging fiber,

22
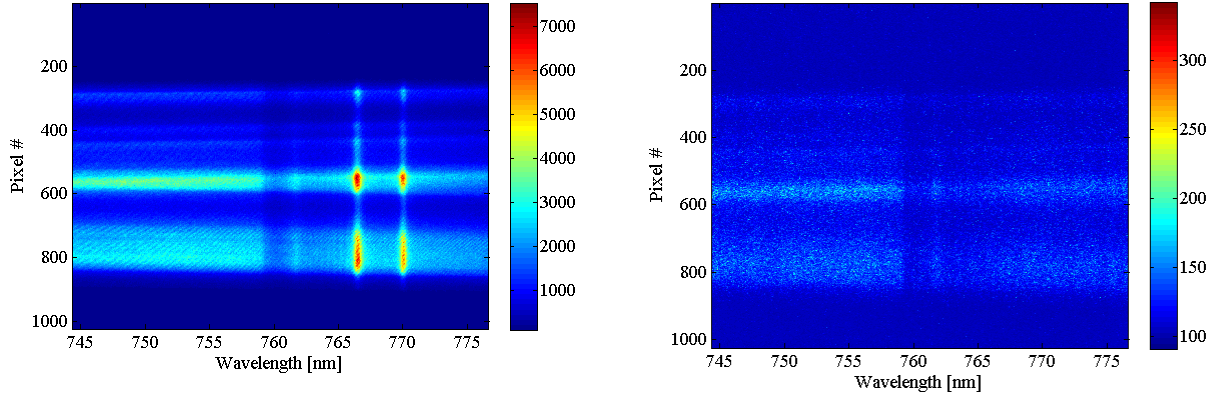
Figure 7. Average of the 10 frames taken in Trial 3 (on the left) of the SRM test and an average of the 10 frames taken with the same settings after the rocket finished burning (on the right.)

this is not possible in this case. The individual fibers in the fiber bundle are arranged simply to bring light from the scene to the spectrometer, not to actually produce an image of the scene. Figure 7 shows the average over ten frames of the raw images for the third trial, as well as, the background measured using the same settings.

First, the ten frames (or the first four for the fourth trial) from each trial were averaged into one image. To determine which rows were completely illuminated by the rocket plume, a histogram of the average intensities across each row was created. The histogram for Trial 3 is shown in Figure 8.
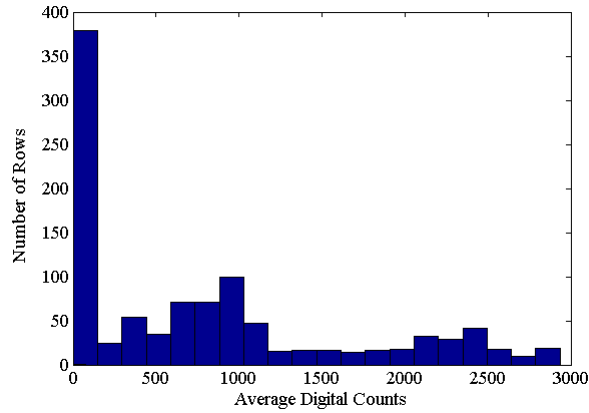
Figure 8. Histogram of average intensity across each row of pixels for Trial 3 of the SRM test.
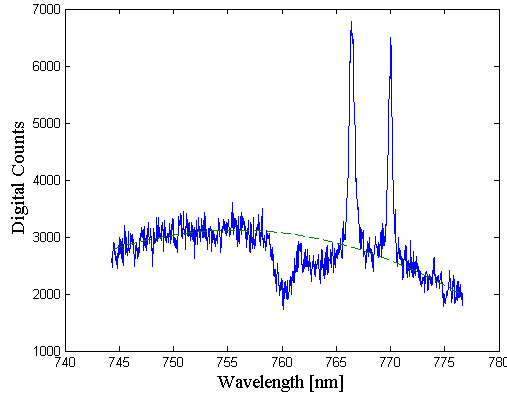
Figure 9. SRM spectrum measured by one row of pixels with the dispersive spectrometer. The baseline fit is also shown.

There is a large spike on the left from the pixels that were totally unilluminated. This is due to the rocket plume not taking up the entire FOV of the telescope. There appears to be two other peaks in the rest of the data. One centered around 1000 DN, and another centered near 2400. These two distributions overlap around 1600 DN. Based on this, a threshold was created to only use rows with average intensity over 1600 to calculate the absorption. The same technique was used to determine the threshold for the first two trials.

It's difficult to say what the first distribution is actually measuring. Since the potassium emission lines are still evident in these rows, the light almost certainly came from the rocket. These rows may correspond to individual fibers in the fiber bundle that are partially illuminated by the rocket plume and partially from the background. This would lead to a lower than expected absorption. The absorption measured for these pixels is lower than the pixels above the threshold used, which supports this idea.

The absorption ratio was then calculated for each row of pixels above the threshold. The spectrum measured by one row of pixels and the baseline fit to the out-of-band points are shown in Figure 9. The error bars were determined by taking the standard deviation of the calculated absorptions. Standard deviation was used, as

24
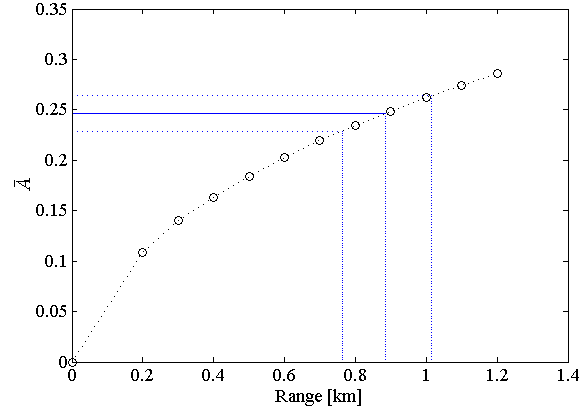
Figure 10. Range estimate with upper and lower bounds based on the absorption measured by the dispersive spectrometer during the SRM test and LBLRTM range curve.

opposed to standard deviation of the mean, to give the error for a single row of pixels. As the experiment is scaled to longer ranges, one or at most a few rows of pixels will be illuminated. The average absorption, with error bounds, was then plotted against the LBLRTM curve of absorption vs. range. A plot of this (again for the third trial) is shown in Figure 10.

These plots do not include the weather correction discussed earlier in this report. The humidity at the time of the rocket firing was 21.3%, the temperature was 27.6 °C, and the pressure was 851.9 hPa. From this data, a concentration of oxygen in the atmosphere can be obtained. LBLRTM gives the concentration it used when predicting the absorption. Based on the weather data, the oxygen concentration used by LBLRTM was about 1.5% too high, so the measured absorptions were multiplied by a factor of 1.015 to compensate for this. Using this correction, range estimates were obtained for each of the four trials. These are summarized in Table **??**.

The true range of 910 m is well within the error bounds for each trial. Additionally, all measured ranges were within 4.5% of the truth value, even when the signal (in digital counts) was very low. This is also encouraging for scaling the experiment to longer ranges, as the irradiance at the detector decreases with range. The telescope

aperture being partially blocked off cut down the number of photons going into the spectrometer, which reduced the SNR.

4.2.1   Comparison to Bomem FTS

A Bomem MR-304 FTS was also taken to this test. It was set to record constantly from five seconds before the rocket ignition to five seconds after it burnt out. A spectrum was taken every 0.1 seconds. An absorption was computed for each frame. Again, the average was taken, while the standard deviation was used as the error. In order to only get the spectra corresponding to time the rocket was actually firing, a threshold was again applied based on average observed intensity. Like before, the results were plotted against LBLRTM to obtain a range estimate as shown in Figure 11.

This provides a range estimate of 920 m, which has comparable accuracy to the dispersive spectrometer. The upperbound was 1.13 km and the lowerbound was 0.74 km. These error bars are much larger than with the dispersive spectrometer. In addition, the absorption measurements are averaged using approximately 60 seconds of data whereas the dispersive spectrometer is only using about 10 seconds of data collection for each trial. Noise has been an issue in the past when using an FTS for passive ranging, so it is encouraging that the dispersive spectrometer gives a less noisy absorption measurement for this test setup.

Table 2. Range estimate summary with error bounds and threshold value used. Range and bounds are reported in km.

Trial	Range	Upper Bound	Lower Bound	Threshold [D.N.]
1	0.89	1.07	0.77	125
2	0.90	1.08	0.75	450
3	0.87	1.00	0.75	1600
4	0.91	1.07	0.77	1600
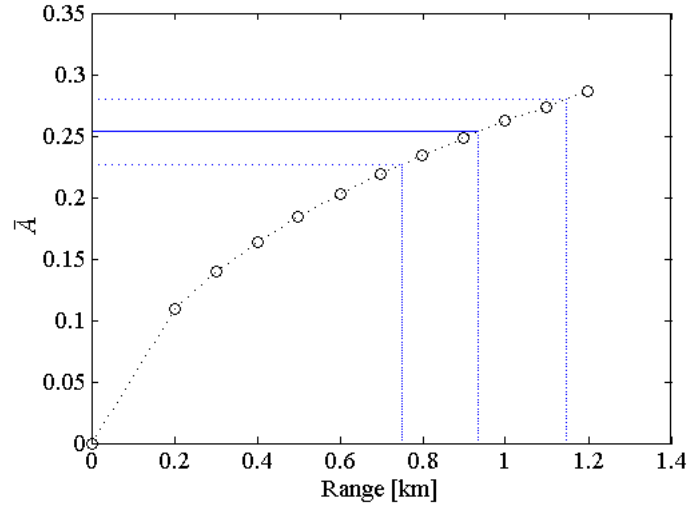
Figure 11. The absorption calculated using the Bomem MR-304 data with upper and lower bounds for the SRM test.

4.3 Hallway Tests

To further characterize this spectrometer, tests were conducted in the hallway of Building 194. The same spectrometer and Meade telescope was used as the Utah test. The source was an Electro-Optical Instruments ISV-410 integrating sphere which uses quartz tungsten halogen lamps. It set to an irradiance of 3000 ft-L. The camera was set to a 0.5 s exposure time and 255 gain. Ten accumulations were used instead of ten frames. This simply adds the counts of ten frames and combines it into one image, as opposed to taking ten separate images. Five trials were taken for each different range. No background was taken because the test was indoors, meaning solar scattering was not an issue. The lights in the hallway were also turned off to minimize the background noise. Both the visible and NIR bands were tested at each range.

Initial testing gave absorption estimates that were consistently higher than those predicted. To troubleshoot this issue, an additional set of data was taken with the source right in front of the telescope. It is expected that there should be no absorption
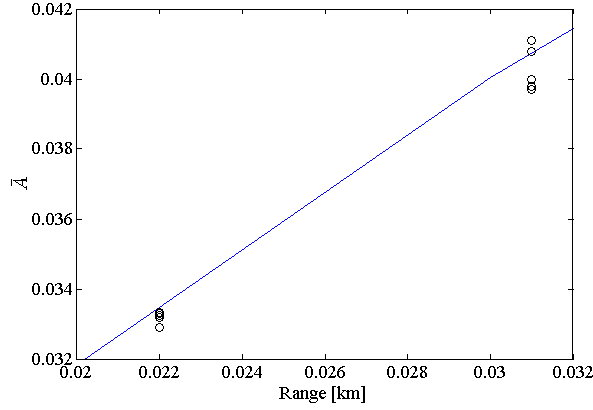
Figure 12. NIR range curve with experimentally measured absorptions.

in this case, but for both the visible and NIR bands, an absorption was measured. It's hard to determine where exactly this is coming from, but it is most likely something inherent in the source. In an integrating sphere, the light will have a relatively long pathlength before actually leaving the source. The measured absoption corresponded to about a 5 m pathlength for the NIR band and a 6 m pathlength for the visible band. Since both bands measure roughly the same atmospheric pathlength, it's very likely something in the source that accounts for this offset. To calculate the actual absorption at a given range, the absorption at 0 range was subtracted from the measured absorptions.

The results for the NIR band measurements are shown in Figure 12. The absorption at 0 m was measured to be 0.0111. For both points, the measured absorption is very close to the predicted. The measured absorption is never further than 0.001 away from the predicted. The measured absorptions at 22 m are all below the predicted absorption. The error, however, translates to less than a meter, so uncertainty in determining the actual range may account for this error.

The visible band data is shown in Figure 13. The measured absorption at 0 m was .00474. In this case the predicted absorption is well within the range of values for each trial, at both ranges. The average for both appears to be slightly off, but
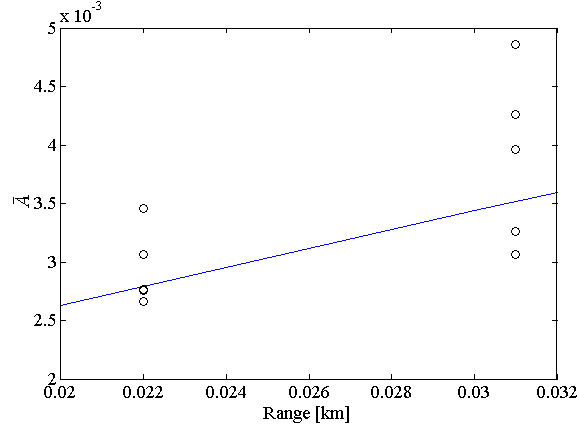
Figure 13. Visible range curve with experimentally measured absorptions.

again this is within a few meters of the truth range. The variation in range estimate between trials is worse than with the NIR band. Since the absorption with the visible band, a fixed error in absorption will produce a larger error in range for the visible band as opposed to the NIR. Since there is less absorption, noise processes such as dark noise will have a greater effect on the measurement.

4.4 Summary

The spectrometer worked very well even at short ranges, so long as the binning feature of the camera wasn't used. The absorption measurement when binning camera pixels was still accurate to within 8%, but the absorption measurement was very noisy. When the camera was not using binning, the measured and predicted absorptions were never more than 5% apart, except when using the visible band at short ranges. This is somewhat expected since the visible band isn't as strong and therefore less effective at short ranges.

V. Filter Data

Another potential method would employ optical bandpass filters, one within the absorption band and two or more outside the band to establish the baseline. This presents several advantages over a spectrometer. First, it would be possible to get a full two dimensional image of the scene, while still obtaining the spectral data. With the dispersive spectrometer, it is only possible to measure one spatial dimension. This means that the target will be easier to track when looking through filters. Secondly, the filters can be custom designed to have a wider bandpass than the individual pixels of the spectrometer. This means a greater irradiance can be measured, which will be advantageous in low light scenarios, such as when the rocket is very far away.

There are some disadvantages to this method, however. First, while each filter will have a greater signal to noise ratio, there will be fewer points to establish a baseline with. So, while the signal to noise ratio in measured intensity will be greater than with the dispersive spectrometer, this doesn't necessarily mean the absorption measurement will be less noisy. This point will be examined further later in this paper. Second, each filter will have to view the same scene. For a dynamic scene, this means it is very difficult to simply take a picture, switch the filter, and take another picture. A potential method for dealing with this will also be discussed later. Finally, it's difficult to make a bandpass filter with a sharp cutoff at both ends of the R-branch. This means that potentially part of the P-branch will be contributing to the measured intensity through the filter. This presents a problem since there will be an increased temperature dependence when only measuring part of the P-branch, which will increase uncertainty. Additionally, the out-of-band region will also be partially within the bandpass of the filter. This can be calibrated for, but it will reduce the sensitivity of the absorption measurement because there is a fixed offset. This means that a small percentage change in the intensity within the absorption

band will correspond to an even smaller percentage change in the intensity measured through the filter.

The camera used for testing was the same PIMAX camera as was used with the spectrometer, but a lens was fit in front of the pixel array. For simplicity, in this testing, the filters were simply placed in front of the camera lens rather than being integrated into the actual optics. There were two separate varieties of filters used in testing, with slightly different sizes. So, it's also important to have an aperture to ensure the detector area is the same, and same number of photons are incident on each filter.

5.1 Filter Functions

The first thing that needs to be done is to determine the spectral response function of the filters. In all, there were 12 filters used in testing for this project. A Cary 5000 UV-Vis-NIR spectral photometer was used to measure the filter transmission. The photometer uses a scanning monochromater and measures the intensity through the filter for a number of different wavelengths. Measurements are taken with the beam completely blocked and completely unimpeded, to establish a calibration. By comparing the measured intensity with these calibrations, the transmission spectrum can be measured. Figure 14 shows the filter functions of all 12 filters used in this paper.

The measured filter transmission at each wavelength is multiplied by the atmospheric tranmission at that wavelength. Figure 15 shows the filter function for the filter in the visible band with no atmospheric absorption overlayed with the filter function combined with atmospheric absorption for a 200 km pathlength with a 45 degree zenith angle. The ratio of the integrated area under the filter function multiplied by the atmospheric transmission to the area under the filter function alone is the
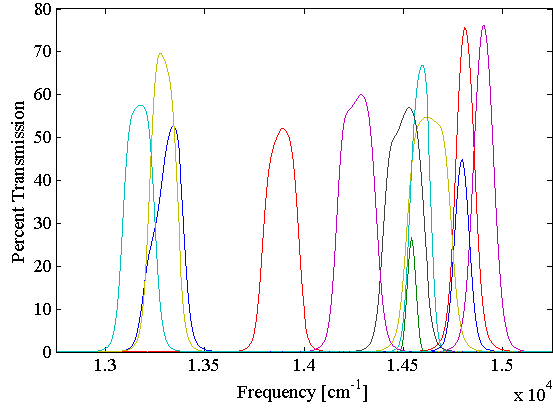
Figure 14. Filter functions for all 12 filters used in testing.

transmission ratio. One minus this is the absorption ratio. This gives the predicted absorptions as a function of range.

When actually measuring absorption, it is also important to determine the filter functions because the filters don't have the same bandwidth. If two filters are centered at the same wavelength, but have different bandwidths, one will measure more digital counts on the camera, despite each measuring the same spectral irradiance. To compensate for this, the integrated area under the spectral response function of each filter was used as a normalization. The digital counts measured by the camera through each filter is divided by this normalization. This normalized intensity was then used to determine the measured absorption.
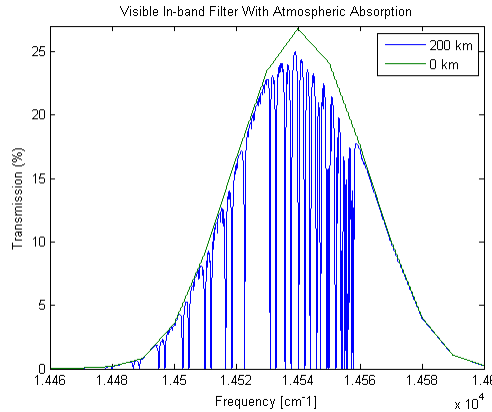
Figure 15. The visible band filter function with no absorption overlayed with the filter function multiplied by the atmospheric absorption through 200 km of atmosphere.

Table 3. Summary of camera and source settings used in hallway filter testing.

Range [m]	Integration Time [s]	Gain [A.U.]	Source Irradiance [ft-L]
24	0.5	175	100
47	0.2	150	300
60	0.4	75	300
82	0.25	100	300
114	0.25	125	300

5.2   Hallway Tests

To determine whether this method can produce accurate range estimates, tests were conducted in the hallway of Building 194 at various distances. The tests were conducted using the same Electro-Optics Integrating Sphere used in the spectrometer hallway tests as the source. Various different camera settings and source irradiances were used based on range, but in every case 25 accumulations were used. This will add 25 frames together to get one image. The camera settings used for each range is summarized in Table 3.

Multiple trials were taken at each range, 2 collections were taken at 47 and 60 m and 3 collections were taken for every other range. Measurements of absorption were taken for both the visible and NIR band. For both bands, the out of band baseline was determined using the filters centered at 675 nm, 700 nm and 752 nm. These were chosen based on having minimal absorption. Since most of the filters were not custom made, they all had at least part of an atmospheric absorption band within their bandpass. The filters chosen to use for fitting a baseline all had absorptions below 3%, even at ranges out to 100 km, so the error this creates should be minimal.

The inband filter used for the NIR band was centered at 760 nm, and was simply an off the shelf filter. As shown in Figure 15, part of its bandpass is outside the R-branch. The filter passes some light which is outside of the oxygen absorption band entirely. This should only affect the data in that it will create a offset in the irradiance

measured through the filters. This should be compensated for since the calculation in LBLRTM also takes this into account. It will, however, limit the dynamic range of the measurement because, even when the band becomes optically opaque, the camera will measure some irradiance. Additionally, part of the filters bandpass is in the P-branch of the absorption band. This could present a problem as the filter only covers part of the P-branch, which will increase the temperature dependence of the absorption measurement. The filters used for the visible band is centered at 687.7 nm and was specifically designed to be used as an inband filter for this band. The wings of the filter function still pass some light outside the R-branch, but it is very minimal. This will be a problem with any filter. It is very difficult to design a filter with a sharp cutoff, because it requires many layers in the filter, which also cuts down on the tranmission within the bandpass.

Because there was some absorption measured even at zero pathlength with the spectrometer, the normalizations used were measured instead of calculated from the filter response functions. To do this, the source was placed right in front of the camera and the intensity was measured through each filter. The digital counts measured by the camera was then used as the normalization factor instead of the integrated area under the filters transmission curve. The new normalized flux is then given as:

$$\Phi_{norm} = \frac{\int T_f(\lambda) \Phi_0(\lambda) a(R) T_a}{\int T_f(\lambda) \Phi_0(\lambda)}. \tag{13}$$

Φ_0 is the flux measured with the source right in front of the camera and $a(R)$ is an attenuation coefficient from the radiometric losses with range. The measured absorption is

$$\bar{A} = 1 - \bar{T} = 1 - \frac{a(R) T_{a,measured}}{a(R) T_{a,baseline}}. \tag{14}$$
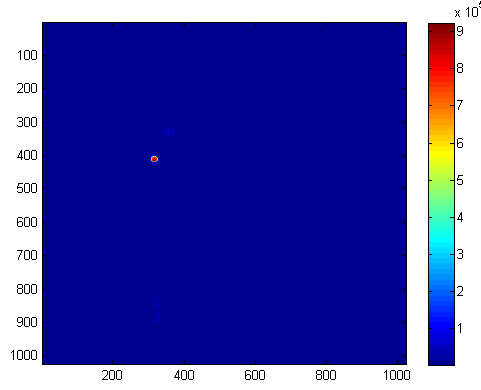
Figure 16. Camera image for a hallway filters test as seen through one filter.

The *a(R)* factor drops out since the radiometric losses are the same for both the baseline and the in-band filter.

Figure 16 shows the picture of the scene taken. From this, it is important to determine which pixels on the camera correspond to the source. To identify these pixels, the brightest pixels were selected. The number of pixels chosen depended on the range and was determined by looking at a plot of the pixels ordered by intensity. A spike is evident for all the pictures and the point approximately half way up the spike is used as the cutoff. An example of this is shown in Figure 17.

For this example, the average digital counts measured by the 250 brightest pixels would be used to calculate the intensity through each filter. This is then divided by the
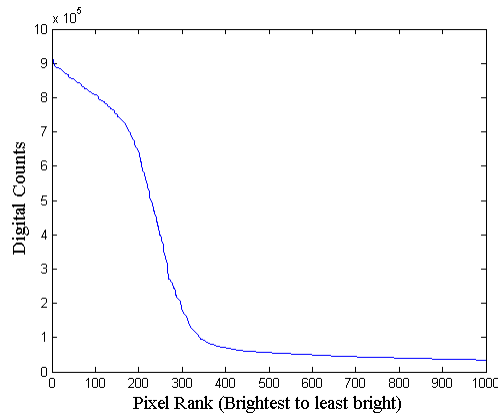
Figure 17. Plot of the thousand brightest pixels, in descending order from a hallway filter test. The cutoff chosen in this case was 250 pixels.
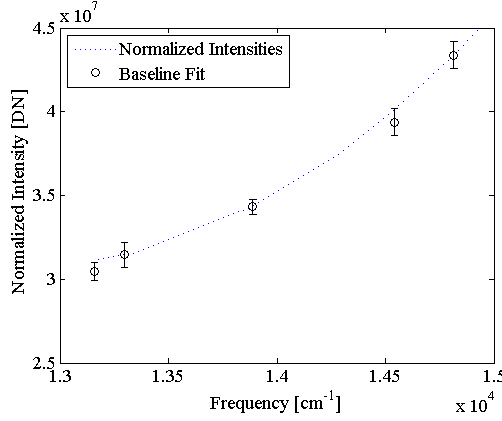
Figure 18. Plot of the normalized intensity measured through each filter observing the lamp at 24 m range. The baseline is fit to the 3 out-of-band filters. The error bars are determined by taking the standard deviation over all pixels above the cutoff.

normalization factor to get a normalized intensity. A baseline is fit to the normalized intensities of the out-of-band filters. The normalized intensity measured through the in-band filter divided by the predicted normalized intensity is the tranmission ratio and one minus the tranmission is the absorption ratio. An example of the normalized intensities measured, along with the baseline fit to the out-of-band points, are shown in Figure 18.

The absorptions measured for the NIR band were all too high, compared to what LBLRTM predicts they should be, by a factor of approximately 2.6. The visible band measurements were too high by a factor of approximately 11.5. The measured absorptions were divided by this factor and the results were plotted with the LBLRTM prediction for absorption versus range. This may be because the normalizations are measured from the source they actually factor out the spectrum of the source. The results are shown in Figure 19.

After dividing by this fixed factor, the predicted absorptions are within the range of the measured absorptions for most cases. The major difficulty with this measurement is it takes time to switch through the filters and collect data. If the source is varying during this time, it will throw the results off. The source is supposed

to provide a stable irradiance, but even small oscillations can throw the absorption measurement off. A plot of how the digital counts vary from frame-to-frame is shown in Figure 20. Clearly the source irradiance, as measured by the camera, is changing with time, which will introduce an error into the absorption measurement.

5.3   Solar Tests

Because a stable source is needed when using filters, the experiment was taken outside to use the sun as a source. In addition, this also gives a longer pathlength, which is advantageous because the ultimate goal of this method is to measure over hundreds of kilometers. In order to do this, a pinhole aperture was used along with a neutral density (ND) filter which reduced the incoming light by a factor of about 8. The ND filter spectral response is assumed to be smoothly varying over the response band. The camera was set to 0.001 s integration time, 0 gain, and 10 accumulations were used. The integrated area under the filter transmission functions were used to normalize the intensities measured through each filter. The spectrum measured is shown in Figure 21.

The measured absorption of the NIR band was 0.270±0.022 while the predicted
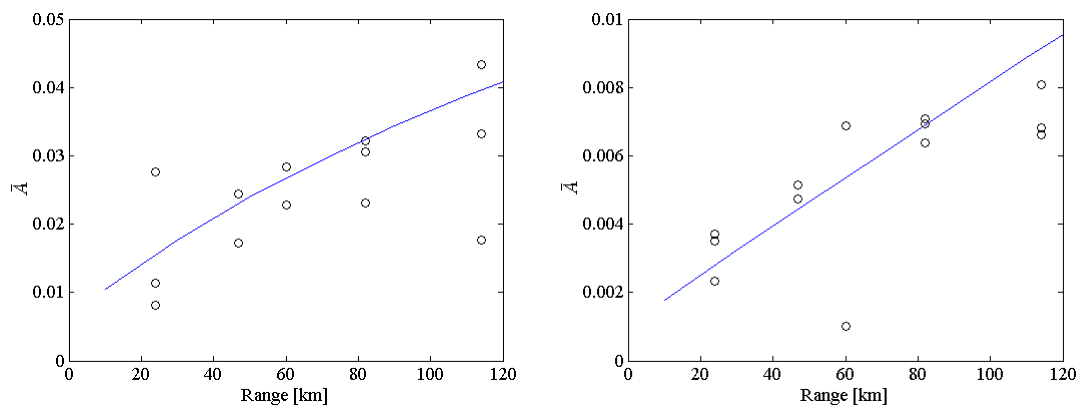
Figure 19. Measured absorptions, with correction applied, plotted with the expected absorptions from LBLRTM in blue. The data for the NIR band is on the left and the visible band is on the right.

37
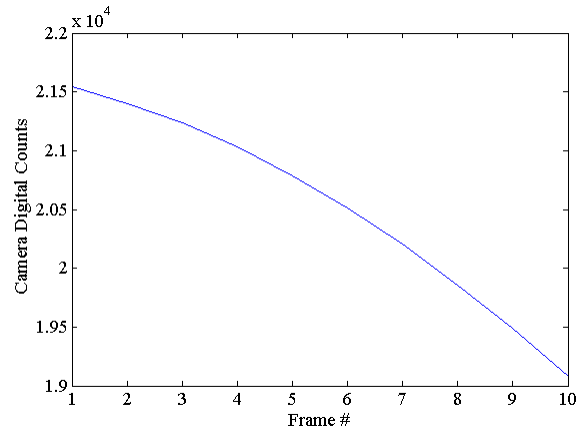
Figure 20. Plot of how the digital counts measured by the camera changes with time looking at the integrating sphere source. A clear trend is visible demonstrating the source is not constant.
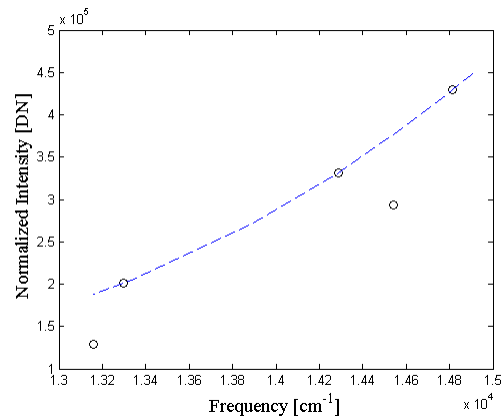
Figure 21. Plot of the normalized intensities measuring the sun through each filter with the baseline fit to the three out-of-band filters used. The two points below the curve are the normalized intensities for the in-band filters. The one on the far left is the NIR band and the one on the right is the visible band.
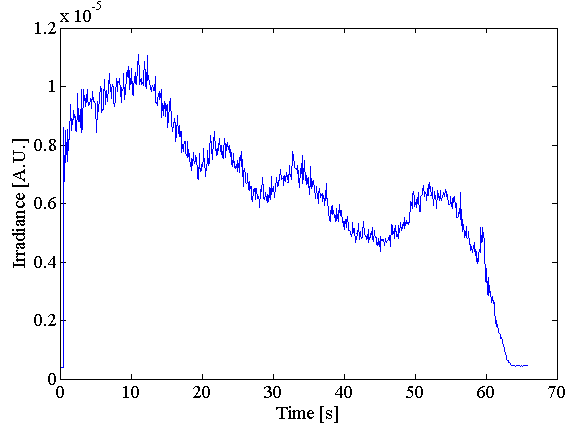
Figure 22. **The average irradiance measured across the entire spectrum plotted vs time. The sharp spike at the beginning and the falloff at the end are due to the rocket starting and finishing it's burn.**

absorption from LBLRTM is 0.266. For the visible band, the measured absorption was 0.176 ±0.025 and the predicted absoption was 0.180. In both cases, the measured absorption is within a couple percent of the predicted which demonstrates using filters to measure absorption can work for a static scene. In reality though, a rocket plume won't be a static source, so simply switching between filters won't work in an operational environment.

5.4 Quad Prism

While simply using the same filters and rotating through them works for static scene, in reality, a real target will have a time varying irradiance. This makes it very difficult to get good data as certain filter intensities will be arbitrarily higher or lower, based on the time they're measured. This is illustrated in Figure 22, which shows the average irradiance across the entire spectrum measured by the Bomem for the SRM observed in Utah versus time. Some of this variation is just noise from the Bomem itself, but there is a clear trend showing the intensity changes as well.

To solve this problem, a quad prism and filter is proposed to simultaneously measure intensity through each filter. The quad prism works much like a Fresnel

biprism where the incoming light is split into separate images. Each image will be the same as the original, but with one fourth the irradiance. If designed correctly, each of these images will appear on a different part of the FPA. By placing a different filter in front of the part of the focal plane corresponding to each image, it is possible to measure the intensity through four filters simultaneously.

To test this idea, a potential system was modeled in ZEMAX, an industry standard optical design and analysis program. The first consideration of such a system is that a field stop is needed before the image is split in four. Without one, parts of each separate image will overlap on the FPA. The light also needs to be collimated going into the prism, otherwise it becomes difficult to separate the images. The prism will also have to be placed at a pupil plane to ensure equal irradiance of each image. Finally, a focusing optic is needed behind the prism to focus the collimated light into an image on the FPA. So, in total, the system will need to consist of 3 optics, in addition to the prism: one to focus the light at the field stop, another to collimate the light before entering the prism, and a third to focus the light on the focal plane.

When modeling the system in ZEMAX, there were a number of considerations for system effectiveness. The system had to be relatively short, on the order of a meter or less, in order to fit on an airborne platform. It also had to have a small enough spot size to adequately image a target that may only be a few pixels.

ZEMAX measures spot size by randomly sending a number of light rays, from the same point in the scene, into the optical system. Then it traces them through to find where they hit on the focal plane. The spot size is the RMS distance of the rays from the center of the spot.

Another important system consideration is the field of view (FOV). The field of view has to be large enough to be able to track a moving target, but also small enough so the rocket plume will correspond to at least a couple pixels, even at long ranges.
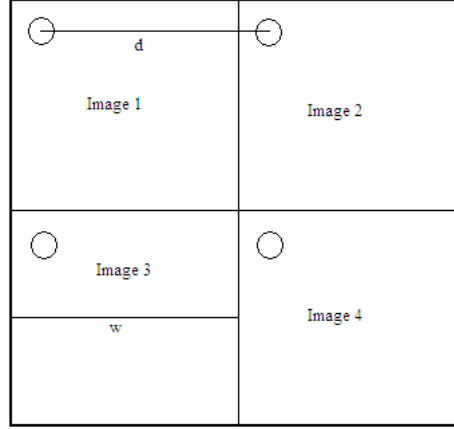
Figure 23. Diagram of the focal plane array which the ideal quad prism system design. The circle is measnt to illustrate an object in the scene being observed.

Along with this, the system has to be designed to separate the images enough to accomodate the field of view. Finally, the system has to have minimal chromatic aberrations to ensure that each pixel will contain all the spectral information of the specific point in the scene.

There are many factors we can adjust to achieve these design goals. The most obvious is the choice of the 3 optics. The first optic will most likely be a telescope of some kind in order to get the necessary angular magnification, as well as, having a large aperture area to collect photons. A reflecting telescope also has the advantage of no chromatic aberration. The other two optics should be lenses, to reduce the system size and complexity. In order to reduce the chromatic aberrations, achromatic doublets will be used. While lenses with short focal lengths will shorten the system, they will also have worse aberrations, so a good balance has to be struck. Another part to consider is the size of the field stop. To ensure the images don't overlap, the field stop will have to be small enough so each separate image will only be a quarter of the entire FPA area, at most. A basic diagram of how the focal plane should be divided is shown in Figure 23.

A final adjustment factor is the wedge angle of the prism. This will determine the angular separation of each image which, along with the focal length of the third

optic, is proportional to the linear separation on the focal plane. The separation of corresponding pixels on the focal plane is given by

$$d \approx 2(n-1)f_3\theta_{wedge}, \tag{15}$$

where n is the index of refraction of the glass, f_3 is the focal length of the lens that focuses the light onto the focal plane, and θ_{wedge} is the wedge angle of the prism. For design, the FPA was assumed to be 1024*1024 pixels, with a 20 micron pixel pitch. This is larger than the pixels of the ICCD used in testing, but 20μm was chosen as a typical value for similar CCDs. This means the FOV has to correspond to approximately 500*500 pixels or 10*10 mm. The size of an individual image on the focal plane, w, is given by

$$w = f_3 FOV_{full} \frac{f_1}{f_2}. \tag{16}$$

Combining this with equation 15, we see that the wedge angle of the prism has to be approximately equal to the full FOV multiplied by the angular magnification of the first two optics.

The system was designed to have a full field of view of 0.1 degrees. At a range of ten km, the FOV is approximately 17*17 m, which is large enough so the width of the rocket plume doesn't completely fill the FOV, making it easier get a background measurement of the scene outside the rocket plume. At a range of 300 km, the FOV of an individual pixel will be one m^2, so the plume will still fully illuminate at least one pixel in most cases. The size of the field stop will be the FOV multiplied by the focal length of the first optic.

For this project, the system was designed to use off the shelf optics for future testing purposes. After modeling several different combinations of lenses, a 1 m focal
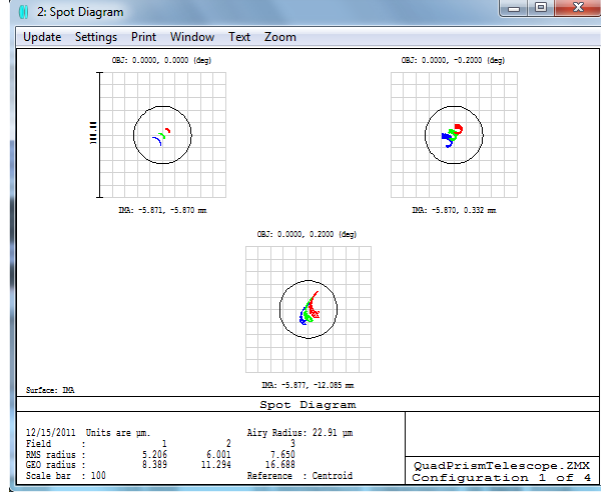
Figure 24. The spot diagram for 3 field angles which actually correspond to a much bigger FOV than the system is designed for. The three colors are for different wavelengths, in this case 750, 760, and 770 nm. Each grid square corresponds to 10x10 microns. The circle respresents the Airy disk, or the diffraction limit of the system.

length f/2 Cassegrain telescope was chosen for the first optic. The second optic was a 100 mm focal length achromatic doublet and the final optic was a 750 mm focal length achromatic doublet. With these optics, the prism wedge angle should be approximately one degree. The field stop will be 1.75*1.75 mm, which is small but not unreasonably small. The overall system length is still over a meter meaning steering mirrors would be necessary to reduce the length of the system. The spot diagram for the system is shown in Figure 24.

Several things can be taken away from the spot diagram. First, the chromatic aberration is essentially negligible, since the differences are all sub-pixel. The spot size is also within the Airy disk, meaning the system is diffraction limited, which is the best case scenario. The diffraction limit is worse than expected for the telescope because the quad prism and the lenses were only two inches in diameter. For production, optics with larger diameters would be desirable. At the edges of the FOV, the spot size gets worse, but at worst it is still sub-pixel.

The ZEMAX software also can determine how much the spot size changes based on errors in the actual assembly of the system. The software computes this by in-

troducing a random amount of error into the positioning and the tilts of each optical element in the system. The maximum amount of error is determined by the tolerances, which are given to the software by the user. The default tolerances are 0.2 mm errors in the positioning of the optics and a 0.2 degree error in the tilt of the optics. A number of different trials are run, and the spot size is measured each time.

In testing this system, the default tolerances were used and 100 different random assemblies were generated based on these errors. The spot size was calculated for each assembly. The average spot radius was 20 microns which means the overall spot size could be a couple pixels. This is a concern since the irradiance would be split over multiple pixels, meaning each pixel will have a lower SNR than if all the energy was focused on one pixel. Additionally, if the target is far enough away to correspond to only one, or a couple, of pixels, irradiance from solar scattering will be mixed with irradiance from the target. This will introduce error into the absorption measurement. Final designs should include tighter assembly tolerances or explore more tolerant designs.

5.5 Summary

Overall, the filter method was very disappointing at short ranges. This is most likely due to the source used in testing, because when a stable source, the sun, was used results were quite accurate. Testing with a stable blackbody would have been ideal, but available blackbodies were not hot enough to give sufficient radiance in the visible and NIR. Testing at long ranges will be difficult as almost any source bright enough to be observed from a few kilometers won't provide a stable irradiance. This is why moving forward the quad prism idea will most likely prove to be the most promising, as it can measure all four filters simultaneously.

VI. Comparison

6.1 SNR and Absorption Error

Since side-by-side testing at long ranges is difficult to arrange, a model was created to predict the SNR performance, and how that translates to error in absorption at long ranges. Based on data from previously measured SRM plumes, the source was modeled as a 2500 K greybody, with emissivity of 0.9, and an area of 5 m^2. The aperture area of the detector was assumed to be 0.1 m^2. A number of different ranges were used to find the relationship between range and absorption error. Additionally, for the spectrometer an additional factor of 0.2 was multiplied in to account for the fiber coupling efficiency. This was chosen based on measured data from the spectrometer both with the fiber, as well as, with the source directly illuminating the entrance slit. Using Equation 8, the number of photons measured by the detector can be calculated once the spectral response functions are added in.

The spectral response functions of individual spectrometer pixels were chosen based roughly on the spectrometer used in the previous tests. The spectral response functions were approximated to be gaussian, with a standard deviation of 0.058 nm, and a normalized peak of 0.3. The spectral separation from pixel to pixel was chosen to match that of the spectrometer, which is approximately 0.032 nm. This was done for 1024 pixels to match the camera, and the same pixels were used for the inband and baseline measurement as was used in testing the spectrometer.

For the filter setup, idealized filters were modeled. The filters were modeled as gaussians. Only the NIR band was examined, so the inband filter was centered at 13145 cm^{-1}, with a full-width at half maximum (FWHM) of 47 cm^{-1}. The out of band filters were centered at 12850, 13300, and 13400 cm^{-1}, all with a FWHM of 118 cm^{-1}. These were chosen to get a minimal overlap with the oxygen and water bands and
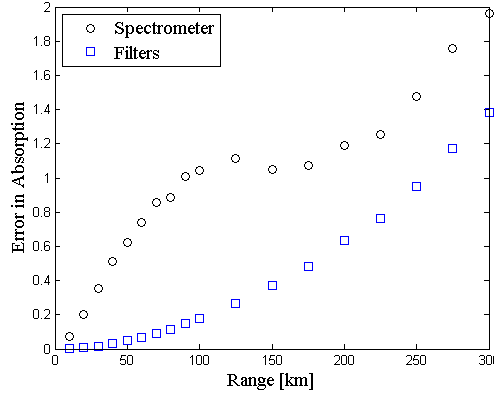
Figure 25. Plot representing the error is absorption of the NIR band vs range for both the filters and dispersive spectrometer based on the model.

also to avoid the potassium emission lines, although this wasn't placed in the model, while still getting the maximum signal possible. Also, the filters were separated as much as possible to get a good sampling for the baseline fit.

By integrating over wavelength with these filter functions, a signal (in number of photons) was predicted for each filter or for each pixel in the spectrometer. The noise was computed by taking the square root of the signal to represent the shot noise, and adding in a constant offset to represent the dark noise. A random number generator was used to multiply the noise by a uniformally distributed, random factor between -1 and 1. This noise value was then added to the signal for each filter or for each pixel of the spectrometer. An absorption was then calculated using the spectrum with the noise introduced. 1000 iterations, each with a randomly generated amount of noise at each point in the spectrum, were used and the standard deviation was taken of the measured absorptions to represent the error. Figure 25 show the results for both the filters and the spectrometer. The NIR band was used with a 95 degree look angle from an altitude of 25 km.

A dip is seen in the middle of the predicted error data for the spectrometer. This is because the sensor is at altitude looking down through the atmosphere. As shown in Figure 3, the absorption increased more rapidly over these ranges, when looking

46

down through the atmosphere. Since this plot shows the ratio of error in absorption to absorption, if the absorption increases rapidly, this ratio is going to be reduced. The reason a leveling off is not visible with the filters is because the filters will measure a lower absorption ratio. This is because in-band filter will measure at least some irradiance outside the band.

This model is mainly meant as a comparison of the two methods with all factors being equal rather than an absolute prediction of range error. It doesn't incorporate some factors, such as the error from solar scattering or source variation, and the noise processes are only estimated.

6.2 Measured SNR Differences

To get a better handle on the actual SNR performance of the filters and spectrometer, more tests were conducted, again with the integrating sphere. Testing was done with the filters and on the spectrometer both with the fiber coupling into it and with the source itself illuminating the entrance slit. In all cases, the source was placed about two feet from the optic, set to 100 ft-L and 10 frames were measured. An absorption was measured for each of the 10 frames averaging across all illuminated pixels, for each frame, and the error was again taken to be the standard deviation of the 10 measured absorption values. The filters gave an absorption error of about 0.027, which is greater than the average absorption measured. The absorption for each frame consistently falls off from one frame to the next. The absorption for each frame is shown in Figure 26. This again demonstrates that the source intensity is changing over the course of the data collection. The quad prism idea would fix this issue.

The spectrometer gave much lower values of error. With the fiber, the error in absorption was 0.0027, which is a tenth of the error measured with the filters. Without
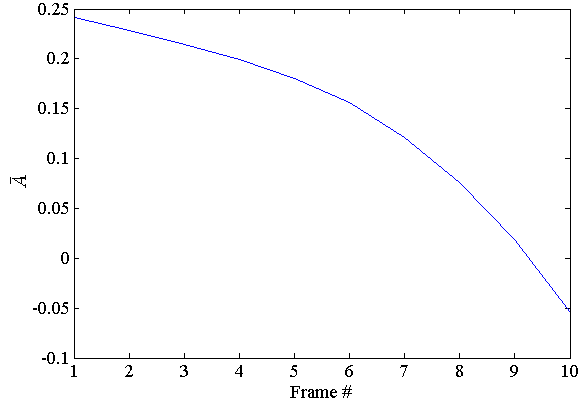
Figure 26. Plots of the measured absorption for each frame using the filters.

the fiber, the error was $4.5*10^{-4}$. If the source is changing with time, this would not affect the spectrometer because the baseline will adjust as well. This is confirmed by looking at the plot of absorption for each frame in Figure 27. Absorption fluctuates randomly and no trend is evident as it was with the filters.

Overall, the performance of the filters at this range is disappointing because there are approximately a million pixels to average over while the spectrometer can only use a couple hundred rows of pixels to average over. Again, this is, at least in part, due to the source varying with time making it difficult to measure with the filters. Another thing learned from this data is that the spectrometer measurements are about 6 times
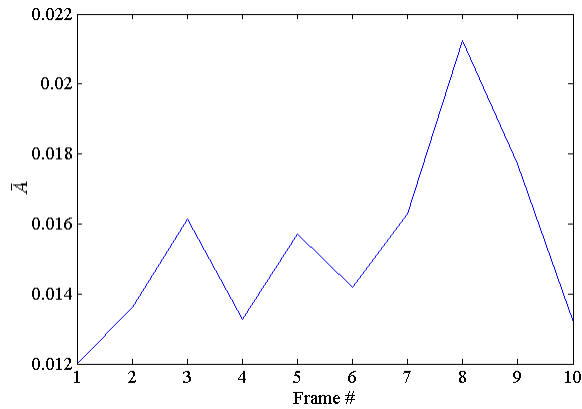
Figure 27. Plots of the measured absorption for each frame using the spectrometer.

48

less noisy without the fiber being used. If possible, it would be best to not use the fiber, when measuring absorption with the spectrometer, in the future.

6.3   Design Considerations

While both of these ideas work in theory, there are issues for both when it comes to actually integrating them into a sensor on an air or space-borne sensor.

6.3.1   Weight

One of the primary concerns is weight. Not only does this affect the other payload on the platform, but it also affects the power needed for motors to actually move the sensor to point at the target. If filters are just going to be rotated in front of a camera, this is a relatively simple and lightweight setup, however, as discussed earlier this presents issues with source intensities that vary with time. The quad filter idea poses some issues when attempting to point at the target, because of the overall length of the system. The optics will also have to be anchored to fairly tight tolerances which will add weight and all of this will be effectively on a lever arm of over a meter. Some sort of beam steering could be employed, such as fiber coupling, from the second optic to the quad prism, or from the telescope to the field stop, although that would require an additional lens to focus the light at the field stop. This will introduce losses in signal, however, the trade off may be necessary because steering the entire system seems impractical.

The dispersive spectrometer will also present some weight issues as there are generally very heavy mountings to secure the mirrors and diffraction grating. The advantage of the dispersive spectrometer, however, is it is a fairly compact design, meaning if it is mounted to the back of a telescope it doesn't need a lot of room to maneuver. Additionally, with a higher groove density grating, the same spectral

dispersion can be accomplished in an even smaller spectrometer. If mounting the spectrometer right to the back of the telescope doesn't work, fiber coupling can be used and still provide effective data as demonstrated earlier, even though again there are losses due to the fiber.

6.3.2 Spectrometer Grating and Length

The spectrometer used in these experiments had only a .275 m pathelength and still gave about 90 pixels within the R-branch of the NIR band, using only a 1200 groove/mm grating. When averaging over the band, 90 pixels is more than enough, so even if the spectral resolution is reduced an accurate measurement of inband intensity can still be made. If the spectral resolution is reduced, this would also allow more out of band points to fit a baseline. It would also be advantageous to trade some spectral resolution as each pixel would have a higher spectral bandwidth, and could therefore measure a greater irradiance. In fact, the spectrometer could even essentially reduce to the filter method, but with more data points, if the spectral resolution is course enough.

6.4 Other Considerations

6.4.1 Rocket and Atmosphere Characterization

Since the spectrometer gives a complete spectrum, it can also be used to measure the water absorption features near both the NIR and visible bands. If properly calibrated, this would give the amount of water in the pathelength. The amount of water in the atmosphere affects the amount of oxygen, so this could be used to develop a more accurate weather correction than simply using weather data at the sensor.

The spectrometer could also measure the potassium emission lines seen earlier

when observing solid rocket motors. By comparing with previously measured specta, this could potentially help classify the specific design of the missile being observed. This could potentially provide information about how to best engage and destroy the target. It would also help in determining what pixels are actually being illuminated by the rocket plume. This could be important when the target is very far away and the effect of solar scattering becomes significant. The filters aren't able to provide this information, since all the out of band points need to be completely isolated from the water absorption and potassium emission to establish a good baseline fit.

6.4.2   Simultaneous Measurement NIR and Visible Bands

The dispersive spectrometer could also provide simultaneous measurements of both the NIR and visible bands. The out of band points used for fitting both bands span from about 12800 cm^{-1} to about 15000 cm^{-1}. If a spectrometer is used with about a quarter of the spectral resolution as the one used in this paper, it would be able to span that range. This would still give about 22 pixels completely within the NIR band and about 20 completely within the visible band. Most of the area in between the two bands is a water absorption feature and thus unsuitable to use for out of band points, but there will still be plenty of points near each absorption feature to fit a baseline to. While this would provide fewer points to fit to, again the measured intensity by each pixel would be greater which would help compensate for the added error in the baseline fit. Since the NIR band absorbs much more strongly, it is better to use at short range, while the visible band is better at long ranges. This design could potentially use both simultaneously to increase accuracy over a greater span of ranges.
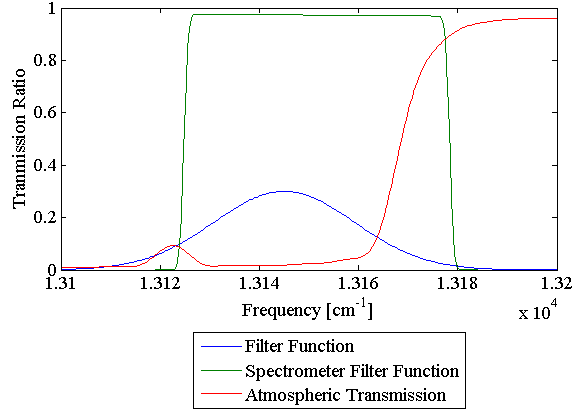
Figure 28. The filter functions used in the model discussed earlier. The spectrometer function represents the sum of the individual filter functions for each inband pixel. The atmospheric transmission is also put in to show the location of the R-branch.

6.4.3 Temperature Dependence

In general, when averaging over the entire R-branch of the absorption band it isn't necessary to worry about the strengths of the individual lines within the branch. The intensities of these lines will change with temperature. When measuring over the entire band these changes are accounted for because every line is averaged. Averaging of the band assumes that the spectral response function is roughly the same across the band, however. This is not the case with the filters as it is very difficult to design a filter with a sharp cutoff, especially over such a short spectral range. The spectrometer is able to give a much more flat spectral response over the band. Figure 28 shows a graph of the spectral response of the filter used in the model from section 6.1. The spectral response of the spectrometer over the band is given by the sum of the gaussians for each pixel within the band. The greater the temperature dependence, the greater the need for an accurate measurement of temperature along the entire pathlength, which is very difficult to obtain.

6.4.4 Tracking

One major disadvantage of the dispersive spectrometer is that it has to image through a slit. This means that the spatial information is limited to one dimension. The width of the FOV will be limited to the FOV of a single pixel. This could make it difficult to point the sensor at the plume and keep it on the target for sufficient time to get an accurate range estimate. If another sensor can be used to obtain tracking information, it may be possible to align the slit with the trajectory of the rocket which will keep it in the sensor FOV longer, without having to constantly move the optics. This may be difficult in practice, however. With the filters, the full two dimensional FOV can be utilized making it easier to find, and track, the target. Both potential designs will probably have to have some sort of secondary sensor to scan the skies and initially identify the rocket, however, as their FOVs are too small to effectively scan the entire sky.

VII.   Conclusions

The spectrometer performed very well in testing with range estimates that were accurate to within tens of meters for ranges up to 900 m. The absorption measured within the NIR when observing a SRM produced a range estimate accurate to within 5% for four separate trials. The spectrometer was also fiber coupled into the telescope for all tests which created an inefficiency and may not be necessary in the future. At ranges on the order of tens of meters, the spectrometer range estimates were accurate to within a meter when measuring the NIR band. Even the visible band at these ranges gave accurate data to within 15 %, although it was somewhat noisy.

Using filters provided less accurate range estimates, however, much of this may be due to the source used in testing. The source used had an irradiance that varied as much as 11%. The filters are much more sensitive to sources with changing irradiances because of the time needed to change between filters. When the sun was used as a source the absorption results were accurate to within 3%, and less noisy. Moving forward, however, will probably require the quad filter idea to be utilized, because the irradiance of rocket plumes will vary with time.

The filters did provide a more accurate range prediction based on a model developed to test both methods for a simple source. The predicted percent error in absorption, as measured by filters, was about half the predicted error when using a dispersive spectrometer. This model only estimated noise processes and did not include other sources of error such as scattering, so absolute predictions of uncertainty can't be made. It appears, however, that all things being equal the filters should provide a more accurate measurement of absorption and thus a more accurate range estimate. This was with idealized filters, however, and a spectrometer design that may not be optimal. For example, if the spectrometer does not have to be fiber coupled to the telescope the spectrometer is predicted to perform better. The spec-

trometer can also be adjusted to measure over a wider wavelength range, which would increase it's predicted SNR. Measured SNR in absorption was far higher when using the spectrometer, as opposed to the filters, even when fiber coupling. Again, at least part of this is most likely due to the source used, however.

Since the spectrometer provides more detailed spectral information it could also be used to simultaneously measure other features as well, which could aid in producing a more accurate weather correction. The spectrometer will be harder to track the target with, however.

Overall, based on testing the spectrometer out performed the filters. The quad prism system, with optimized filters, should improve the performance of the filters method. The spectrometer, however, will still give more detailed spectral data which could be used to produce better weather corrections. Also, a spectrometer can also be made with coarse enough spectral resolution that it essentially becomes the filter method, but with more than just three out-of-band points.

7.1 Future Work

The biggest area for further development of these techniques is to test them at larger distances from the source. For this testing, pathlengths of up to nearly a kilometer were used, but this technique is designed for ranges up to hundreds of kilometers. The filters were tested using the sun as a source which is a long atmospheric pathlength, but the sun is also a much more luminous source than any rocket plume.

Additionally, all the targets looked at were stationary sources. By looking at moving targets, issues such as tracking the target can be examined, as well as, how the source moving across the FOV affects the intensity measured by each camera pixel. Code would also need to be developed to compute a range estimation in near real time. To implement in a sensor, a range will have to be determined within

seconds of the actual measurements of the source. So far, the data analysis has all been done by hand, which will need to be changed. This has been done successfully in the past with an FTS, but not using the instruments used in this paper. [9]

The quad prism idea was examined in principle, but the quad filter needs to be custom made to test the idea experimentally. Changes in the source irradiance appear to affect the filter method, it would be desirable to find out whether fixing this with the quad prism will lead to less noisy absorption measurements using filters. Also, it will have to be examined how the system truely performs from an aberration standpoint, based on errors in the actual assembly.

In this testing, only one grating was used because it was the only one blazed near the spectral region measured. If different gratings are used, the spectrometer can be tested with different spectral resolutions. This would help determine the trade off between having a lot of points to fit a baseline to and having enough signal at each point. Additionally, different gratings would allow the water absorption band in between the NIR and visible O_2 bands. This could potentially allow the amount of water in the pathlength to be determined which would allow for a better weather correction.

Another potential idea is to use the spectral lines for different isotopes of oxygen and measure absorption based on those lines. Since these isotopes are much more rare than the $^{16}O^{16}O$ molecule, they can have even longer pathlengths before saturating. The disadvantage of this method is it needs very high spectral resolution to be able to distinguish these lines from the $^{16}O^{16}O$ oxygen lines. This level of spectral resolution means the band cannot be measured all at once, meaning there will be a very large dependence on temperature along the entire path. It is difficult to get accurate weather data along the entire pathlength, so this will create an uncertainty. Also, the

spectral irradiance from the target will be smaller, since such a small region of the spectrum is being examined.

Appendix A. MATLAB Code Used

%%%%%% CALCULATE ABSORPTION BASED ON CAMERA DATA FOR FILTERS

%Filters used in testing

filters=[6700,6750,6860,6877,6900,7000,7200,7500,7520,7600];

%% Import image files [filen,pnm]=uigetfile({'*.txt','*.dat'},'MultiSelect', 'on','Choose Image Files');

for j=1:length(filters);

fnm=cell2mat(filen(1,j));

filename=fullfile(pnm,fnm);

dat=csvread(filename);

[rr,cc]=size(dat);

Nrow=dat(rr,2); % number of camera rows

userows=1:Nrow;

avgim(:,:,j)=dat(userows,(3:1026));

end

%% Import background images

[filenb,pnmb]=uigetfile({'*.txt','*.dat'},'MultiSelect', 'on','Choose Background Files');

for j=1:length(filters);

fnmb=cell2mat(filenb(1,j));

filenameb=fullfile(pnmb,fnmb);

datb=csvread(filenameb);

[rr,cc]=size(datb);

Nrow=datb(rr,2); % number of camera rows

userows=1:Nrow;

avgimb(:,:,j)=datb(userows,(3:1026));

end

%% Compute normalized intensities

for i=1:length(filters);

%select N brightest pixels (pixels corresponding to actual source)

N=10;

im=(avgim(:,:,i)-avgimb(:,:,i));

% Creates an array of intensity measured for each filter.

image=sort(im(:),'descend');

toppix=image(1:N);

intensity(i)=mean(toppix);

end

% Normalize measured intensity by area under filter function

normint=intensity./norm;

%% Calculate Absorption

% Out-of-Band Filters Used

obfused=[2,3,9];

wn=10^8./filters;

nu_out=wn(obfused);

% In-band Filter Function Centers

nu_in=10^8/7600; % NIR band

%nu_in=10^8/6877; % Visible band

% Create baseline and absorption

basefit=polyfit(nu_out,normint(obfused),2);

baseline=polyval(basefit,nu_in);

Abar=(baseline-normint(length(filters)))/baseline; % NIR band

%Abar=(baseline-normint(find(filters==6877)))/baseline; % Visible band

%%%%% CALCULATE PREDICTED ABSORPTION VS. RANGE CURVE (FILTERS)

%% Import Inband filter [fnm,pnm]=uigetfile({'*.csv','*.dat'},'Import In-band Filter');

filename=fullfile(pnm,fnm);

data=dlmread(filename,',',[2 0 1599 1]);

dat=data(1:length(data(:,1))-2,:);

%% LBLRTM Run

clear T R A

% Set up path path(pwd,path);

if ~exist('LBLRTM_DIR','var'); [LBLRTM_DIR,LBLCODE,OUT_DIR]=setglobals; end

res=8;

ff=dat(:,1);

filterT=dat(:,2);

MOPD=1/res;

nu_cen=10^8/(data(length(dat)+1,1));

nu_min=nu_cen-750;

nu_max=nu_cen+750;

R =[.01:.02:.21]; % Range values to iterate through

for j=1:length(R);

disp(' '); disp(['— For R=',num2str(R(j)),' km —']); lblrtm = gen_TP5_struct('pathlength',R(j),'Alt 'ZenithAngle',87,'nu_max',nu_max,'nu_min',nu_min,'MOPD',MOPD,'apodizer','tri',... 'MODEL',6);

[f,trans] = compute_transmittance_hi(lblrtm);

T(:,j)=trans(:);

end

filterThigh=interp1(ff,filterT,f,'linear');

for j=1:length(R);

int(j)=trapz(filterThigh'.*T(:,j));

end

figure(1);

plot(f,filterThigh'.*T(:,1));

A=1-int/trapz(filterThigh);

figure(2);

plot(R,A);

title('Absorption vs. Range Curve');

xlabel('Range [km]'); ylabel('Absorption Ratio')

%%%%% MODEL SNR FOR FILTERS

%% Compute atmospheric transmission

clear lblrtm R T Abar

% Set up path path(pwd,path);

if ~exist('LBLRTM_DIR','var'); [LBLRTM_DIR,LBLCODE,OUT_DIR]=setglobals;

end

% set up band to compute

nu_min=12400;

nu_max=13900;

res = 8; % in wavenum

MOPD = 1/res; % in cm

f = nu_min:(1/MOPD):nu_max;

% compute transmission for several different ranges

R = [10:10:90,100:25:300]; % Range values to iterate through

```
for j=1:length(R);

disp(' '); disp(['— For R=',num2str(R(j)),' km —']); lblrtm = gen_TP5_struct('pathlength',R(j),'Alt
'ZenithAngle',95,'nu_max',nu_max,'nu_min',nu_min,'MOPD',MOPD,'apodizer','tri',...
'MODEL',6);

[f,trans] = compute_transmittance_hi(lblrtm);

T(:,j)=trans(:);

end

figure(1);

plot(f,transpose(T(:,18)));

%% Model target as greybody function

h=6.626*10^-34;

c=3*10^8;

k=1.38*10^-23;

t=2500;

eps=.9;

BB=eps*2*10^6*c*f.^2.*(1./(exp(100*h*c*f/(k*t))-1));

%% Create model filters

nu=[13145 12850 13300 13400]; % Filter Centers (inband first)

inband=20; % Inband filter width

outband=50; %Outofband filter width

for i=1:4;

if i==1;

filters(:,i)=.3*exp(-((f-nu(i)).^2)/inband^2);

else filters(:,i)=.5*exp(-((f-nu(i)).^2)/outband^2);

end

end
```

```matlab
for j=1:length(R);

for i=1:4;

int(i,j)=trapz(filters(:,i).*T(:,j).*BB');

end

end

%% Calculate signal and noise at detector

ar=5; % Area of the Plume (in m^2)

sa=ar./(R*1000).^2; % Solid Angle Subtended by the Plume

aa=.1; % Aperture Area (in m^2)

pix=1024*(2./.1*(pi/180)*R*1000).^2; % Number of pixels rocket plume corre-
```
sponds to
```matlab
QE=0.5; % Quantum Efficiency

inttime=0.001; % Camera Integration Time

for j=1:length(R);

for i=1:4;

signal(i,j)=int(i,j)*QE*sa(j)*aa*inttime/4;

end

end

for j=1:length(R);

for i=1:4;

noise(i,j)=(sqrt(signal(i,j))/pix(j))+108;

end

end

%% Calculate Absorption Error

for k=1:1000;

clear basefit baseline count
```

% Add or subtract random amount of noise to signal

for j=1:length(R);

for i=1:4; count(i,j)=signal(i,j)+2*(rand()-.5)*noise(i,j);

end

end

% Create baseline and calculate absorption

for j=1:length(R);

basefit=polyfit(nu(2:4)',count(2:4,j),2);

baseline=polyval(basefit,nu);

warning off all

Abar(j)=(baseline-count(1,j))/baseline;

A(j,k)=Abar(j);

end

end

% Find variation in absorption measurements

for j=1:length(R)

error(j)=std(A(j,:));

end

figure(1);

plot(R,(error./mean(A,2)')*100);

xlabel('Range[km]'); ylabel('Percent Error in Absorption');

title('Percentage Error in Absorption vs Range (NIR filters)');

%%%%%% MODEL SNR FOR SPECTROMETER

%% Compute atmospheric transmission

clear lblrtm R T Abar

% Set up path path(pwd,path);

```matlab
if ~exist('LBLRTM_DIR','var'); [LBLRTM_DIR,LBLCODE,OUT_DIR]=setglobals;
end
    % set up band to compute
    nu_min=12800;
    nu_max=13500;
    res = 8; % in wavenum
    MOPD = 1/res; % in cm
    f = nu_min:(1/MOPD):nu_max;
    % compute transmission for several different ranges
    R = [10:10:90,100:25:300]; % Range values to iterate through
    for j=1:length(R); disp(' '); disp(['— For R=',num2str(R(j)),' km —']); lblrtm =
gen_TP5_struct('pathlength',R(j),'Altitude',25,... 'ZenithAngle',95,'nu_max',nu_max,'nu_min',nu_min,'
'MODEL',6);
    [f,trans] = compute_transmittance(lblrtm);
    T(:,j)=trans(:);
    end
    figure(1);
    plot(f,transpose(T(:,18)));
    %% Model target as greybody function
    h=6.626*10^-34;
    c=3*10^8;
    k=1.38*10^-23;
    t=2500;
    eps=.9;
    BB=eps*2*10^6*c*f.^2.*(1./(exp(100*h*c*f/(k*t))-1));
    %% Create model filters
```

```matlab
wav=linspace(776.6584,744.3316,1024); % Pixel Centers (in nm)

nu=1./(wav*10^-7); % Pixel Centers (in wavenumbers)

bw=1; % Pixel Bandwidth

for i=1:1024;

filters(:,i)=.3*exp(-((f-nu(i)).^2)/bw^2);

end

for j=1:length(R);

for i=1:1024;

int(i,j)=trapz(filters(:,i).*T(:,j).*BB');

end

end

%% Calculate signal and noise at detector

ar=5; % Area of the Plume (in m^2)

sa=ar./(R*1000).^2; % Solid Angle Subtended by the Plume

aa=.1; % Aperture Area (in m^2)

fe=.2; % Fiber coupling efficiency

pix=1024*2./(.1*(pi/180)*R*1000); % Number of pixels rocket plume corresponds
```

to

```matlab
QE=0.5; % Quantum Efficiency

inttime=0.001; % Camera Integration Time

for j=1:length(R);

for i=1:1024; signal(i,j)=int(i,j)*QE*sa(j)*aa*fe*inttime;

end

end

for j=1:length(R);

for i=1:1024;
```

```
noise(i,j)=sqrt(signal(i,j))./sqrt(pix(j))+10^8;

end

end

%% Calculate absorption error

obpix=[1:100,600:1000]; % Out of band pixels

ibpix=[474:565]; % In band pixels

for k=1:1000;

clear basefit baseline count

% Add or subtract random amount of noise to signal

for j=1:length(R);

for i=1:1024;

count(i,j)=signal(i,j)+2*(rand()-.5)*noise(i,j);

end

end

% Create baseline and calculate absorption

for j=1:length(R);

basefit=polyfit(nu(obpix)',count(obpix,j),3);

baseline=polyval(basefit,nu(ibpix));

warning off all

Abar(j)=mean((baseline-count(ibpix,j)')./baseline);

A(j,k)=Abar(j);

end

end

% Find variation in absorption measurements

for j=1:length(R)

error(j)=std(A(j,:));
```

end

figure(1);

plot(R,(error./mean(A,2)')*100);

xlabel('Range[km]'); ylabel('Percent Error in Absorption');

title('Percentage Error in Absorption vs Range (NIR Spectrometer)');

%%%%%%% CALCULATE MEASURED ABSORPTION BASED ON CAMERA DATA FOR SPECTROMETER

%Import image file

[fnm,pnm]=uigetfile({'*.txt','*.dat'},'Choose ASCII file');

filename=fullfile(pnm,fnm);

dat=csvread(filename);

[rr,cc]=size(dat);

Nfrm=dat(rr,1); % number of frames recorded

%Nfrm=4; % Trial 4 only had 4 frames with the rocket burning

Nrow=dat(rr,2); % number of camera rows

pix=(1:1024);

int=zeros(Nrow,1024,Nfrm);

for frm=1:Nfrm;

userows=(1:Nrow)+(Nrow*(frm-1));

int(:,:,frm)=dat(userows,(3:1026));

end

figure(1);

avgim=mean(int,3);

imagesc(pix,pix,avgim); colorbar;

xlabel('Pixel #'); ylabel('Pixel #')

title([fnm,' (avg over ',num2str(Nfrm),' frames)']);

%Import background image file

[fnmb,pnmb]=uigetfile({'*.txt','*.dat'},'Choose Background file');

filenameb=fullfile(pnmb,fnmb);

datb=csvread(filenameb);

[rr,cc]=size(datb);

Nfrm=datb(rr,1); % number of frames recorded

Nrow=datb(rr,2); % number of camera rows

intb=zeros(Nrow,1024,Nfrm);

for frm=1:Nfrm;

userows=(1:Nrow)+(Nrow*(frm-1));

intb(:,:,frm)=datb(userows,(3:1026));

end

figure(2);

avgimb=mean(intb,3);

imagesc(pix,pix,avgimb); colorbar;

xlabel('Pixel #'); ylabel('Pixel #')

title([fnm,' (avg over ',num2str(Nfrm),' frames)']);

%% Absorption Calculation

% Iterate through each row of camera data

for n=1:1024;

f=1:1024;

T=avgim(n,:)-avgimb(n,:); % Intensity at each pixel along a row

%create threshold based on average intensity across a row weight(n)=mean(T);

% Trial 1: weight¿125

% Trial 2: weight¿450

% Trial 3&4: weight¿1600

```
if weight(n)¿1600;

thresh(n)=1;

else thresh(n)=NaN;

end

% Define in and out-of-band limits

i_bnds=[1,100,474,565,600,1000];

% clip out an array of only the out-of-band Transmission data

ii=[i_bnds(1):i_bnds(2),i_bnds(5):i_bnds(6)];

Tout=T(ii); Tout=Tout';

fout=f(ii); fout=fout(:);

% Now clip the in-band part to use in finding band avg

fR = f(i_bnds(3):i_bnds(4));

TR = T(i_bnds(3):i_bnds(4));

Ar=zeros(length(TR));

% Fit baseline to out-of-band data and measure absorption

basefit=polyfit(fout,Tout,2);

baselineR=polyval(basefit,fR);

Ar=1-TR./baselineR;

ARbar(n)=trapz(Ar);

end

% Normalize

ARbar=ARbar./length(fR);

avgabs=nanmean(ARbar.*thresh);

% Standard deviation or standard deviation of the mean

error=nanstd(ARbar.*thresh);

%error=nanstd(ARbar.*thresh)/sqrt(numel(find(isfinite(thresh))));
```

%%%%%% CALCULATE PREDICTED ABSORPTION VS. RANGE CURVE (SPECTROMETER)

%% Calculate Atmospheric Transmission

clear lblrtm R T Abar

% Set up path path(pwd,path);

if ~exist('LBLRTM_DIR','var'); [LBLRTM_DIR,LBLCODE,OUT_DIR]=setglobals;
end

% set up band to compute

nu_min=12700;

nu_max=13300;

res = 8; % in wavenum

MOPD = 1/res; % in cm

f = nu_min:(1/MOPD):nu_max;

% compute transmission for several different ranges

R = [0.2:0.1:1.2]; % Range values to iterate through

for j=1:length(R);

disp(' '); disp(['— For R=',num2str(R(j)),' km —']);

lblrtm = gen_TP5_struct('pathlength',R(j),'Altitude',1.495,... 'ZenithAngle',96.7,'nu_max',nu_max,' 'MODEL',6);

[f,trans] = compute_transmittance(lblrtm);

T(:,j)=trans(:);

end

figure(1);

plot(f,T(:,10)');

%% Find Predicted Absorption

% Out-of-band limits

```matlab
basefreq=[12750,12900,13200,13400];

for j=1:length(basefreq);

err=abs(f-basefreq(j));

ilim(j)=find(err==min(err),1);

end

base_i=[(ilim(1):ilim(2)),(ilim(3):(ilim(4)))];

% In-band limits

inbandf=[13122,13170];

for j=1:length(inbandf);

err=abs(f-inbandf(j));

ilim(j)=find(err==min(err),1);

end

band_i=(ilim(1):ilim(2));

% Fit baseline and measure absorption

Abar=zeros(size(R));

for j=1:length(R); % find baseline by fitting to out of band data

warning('off','MATLAB:polyfit:RepeatedPointsOrRescale');

basefit=polyfit(f(base_i)',T(base_i,j),2);

baseline=polyval(basefit,f);

A=1-( T(band_i,j)./baseline(band_i)' );

Abar(j)=trapz(A)/length(band_i);

end

figure(2)

plot([0,R],[0,Abar],'ko:');

hx=xlabel('Range [km]'); hy=ylabel('$\bar{A}$','Interpreter','latex');

ht=title('LBLRTM Result for ATK (8 cm^{-1} sampling)');
```

```
set([gca,hx,hy,ht],'FontName','Times','FontSize',14)
```

%% Find Range based on predicted absorptions

```
x=linspace(0,1.2,100);
```

```
calculatedA=zeros(1,100);
```

```
calculatedAu=zeros(1,100);
```

```
calculatedAl=zeros(1,100);
```

% Create array for measured absorption as well as upper and lower bounds % based on error

```
for j=1:100
```

```
calculatedA(j)=avgabs;
```

```
end
```

```
for j=1:100
```

```
calculatedAu(j)=avgabs+error;
```

```
end
```

```
for j=1:100
```

```
calculatedAl(j)=avgabs-error;
```

```
end
```

% Find where average absorption and error bounds intersect with the LBLRTM generated absorption vs. range curve [xi,yi]=polyxpoly(R,Abar,x,calculatedA);

```
[xiu,yiu]=polyxpoly(R,Abar,x,calculatedAu);
```

```
[xil,yil]=polyxpoly(R,Abar,x,calculatedAl);
```

```
rangeestimate=xi
```

```
upperbound=xiu
```

```
lowerbound=xil
```

```
figure(3);
```

```
plot([0,R],[0,Abar],'ko:',[linspace(0,xi,100)],calculatedA,'b',[linspace(0,xiu,100)],calculatedAu,'b:',[li
```

hx=xlabel('Range [km]'); hy=ylabel('$\bar{A}$','Interpreter','latex');

ht=title({'Range Estimate With Upper and Lower Bounds';'(Pixels Above Thresh-old)'});

set([gca,hx,hy,ht],'FontName','Times','FontSize',14)

Bibliography

[1] G.D. Boreman E.L. Dereniak. *Infrared Detectors and Systems.* John Wiley & Sons Inc., 1996.

[2] Michael T. Eismann. *Hyperspectral Remote Sensing.* SPIE Press, 2012.

[3] Norman K. Leonpacher. Passive infrared ranging. Master's thesis, Air Force Institute of Technology, 1983.

[4] C. K. Chuang Matt Hanson Larry Lillard Brian Hibbeln James S. Draper, Sumner Perlman and Darren Sene. tracking and identification of distant missiles by remote sounding. *Proceedings of IEEE Aerospace Applications Conference*, 4:333–341, 1999.

[5] Nahum Gat Gordon Scriven. Advanced monocular passive ranging (ampr) for halo ii. Technical report, AFRL, March 2008.

[6] Michael R. Hawks. *Passive Ranging Using Atmospheric Oxygen Absorption Spectra.* PhD thesis, Air Force Institute of Technology, 2005.

[7] Douglas J. Macdonald. Passive ranging using infra-red atmospheric attenuation. Master's thesis, Air Force Institute of Technology, 2010.

[8] Joel R. Anderson. Monocular passive ranging by an optical system with band pass filtering. Master's thesis, Air Force Institute of Technology, 2010.

[9] R. Anthony Vincent. Passive ranging of dynamic rocket plumes using infrared and visible oxygen attenuation. Master's thesis, Air Force Institute of Technology, 2011.

[10] Gerhard Herzberg. *Molecular Spectra and Molecular Structure, vol I: Spectra of Diatomic Molecules.* Van Nostrand Reinhold, 1998.

[11] Spectralcalc line list browser.

[12] P. D. Brown S. Boukabara K. Cady-Pereira M. J. Iacono J. S. Delamere S. A. Clough, M. W. Shephard and E. J. Mlawer. Atmospheric radiative transfer modeling: a summary of the aer codes. *Journal of Quantitative Spectroscopy and Radiative Transfer*, 91:233–244, 2005.

[13] Joseph Ladislas Wiza. Microchannel plate dete. *Nuclear Instruments and Methods*, 162:587–601, 1979.

[14] Paul R. Yoder Robert E. Fischer, Biljana Tadic-Galeb. *Optical System Design.* SPIE, 2008.

REPORT DOCUMENTATION PAGE

1. REPORT DATE *(DD–MM–YYYY)*	2. REPORT TYPE	3. DATES COVERED *(From — To)*
20–12–2012	Master's Thesis	1 Sep 2010 - 20 December 2012

4. TITLE AND SUBTITLE	5a. CONTRACT NUMBER
Passive Ranging Using a Dispersive Spectrometer and Optical Filters	5b. GRANT NUMBER
	5c. PROGRAM ELEMENT NUMBER

6. AUTHOR(S)	5d. PROJECT NUMBER
	13P191
	5e. TASK NUMBER
Jacob A. Martin	
	5f. WORK UNIT NUMBER

7. PERFORMING ORGANIZATION NAME(S) AND ADDRESS(ES)	8. PERFORMING ORGANIZATION REPORT NUMBER
Air Force Institute of Technology Graduate School of Engineering and Management (AFIT/EN) 2950 Hobson Way WPAFB OH 45433-7765	AFIT-ENP-12 − D − 02

9. SPONSORING / MONITORING AGENCY NAME(S) AND ADDRESS(ES)	10. SPONSOR/MONITOR'S ACRONYM(S)
intentionally left blank	11. SPONSOR/MONITOR'S REPORT NUMBER(S)

12. DISTRIBUTION / AVAILABILITY STATEMENT

APPROVED FOR PUBLIC RELEASE; DISTRIBUTION UNLIMITED.

13. SUPPLEMENTARY NOTES

14. ABSTRACT

Monocular passive ranging using atmospheric oxygen absorption has been demonstrated in the past using an FTS. These instruments are very sensitive to vibration making them difficult to use on an airborne platform. This work focuses on whether passive ranging can be done with instruments that are easier to deploy. Two potential instruments are tested and compared: a diffraction grating spectrometer and optical filters. A grating spectrometer was able to estimate range to within 5% for a static solid rocket motor firing at a distance of 910 m using the NIR absorption band of oxygen. Testing at shorter ranges produced range estimates accurate to within 5% for the NIR band and 15% for the visible band. Using the sun as a source, optical filters were able to successfully measure the pathlength through the atmosphere to within 3% for both bands. Testing the filters using a quartz lamp as the source, however, proved unsuccessful. A system is discussed and modeled in ZEMAX to potentially measure multiple filters simultaneously. A model was also created to predict how both techniques will scale to longer ranges. Using filters is predicted to be more accurate at long ranges, but only if the grating spectrometer has to be fiber coupled to the collection optic.

15. SUBJECT TERMS

Monocular Passive Ranging, Band Averaged Absorption, Rocket Plume Emission, Atmospheric Absorption Bands, Radiative Transfer Modeling

16. SECURITY CLASSIFICATION OF:			17. LIMITATION OF ABSTRACT	18. NUMBER OF PAGES	19a. NAME OF RESPONSIBLE PERSON
a. REPORT	b. ABSTRACT	c. THIS PAGE			Lt Col Michael R. Hawks, AFIT/ENP
U	U	U	UU	89	19b. TELEPHONE NUMBER *(include area code)* (937)255-3636 x4828; michael.hawks@afit.edu